first TV peak at puberty is significantly smaller than those that occur thereafter. The amplitude of seasonal cyclicity and baseline volume becomes higher as animals mature. The concentration of T increases from 4 to 7 years with considerable fluctuation due to seasonality. Individual variation is substantial in terms of age at T peak and TV peak but, as the cyclicity and amplitude correspond closely among individuals, the cross-sectional diagram preserves the seasonal effect (Fig. 1b).

The relationship between TV and T level was quite tight in each of the individuals, but there was a slight lag between T peak and TV increase in the period where TV had not yet attained maturity (see Fig. 4). Matsubayashi and Enomoto (1983) reported for adult Japanese macaques that the T level increases rapidly from July to attain a peak in September, and that the TV peak is found in October. Their result appears to show a lag between T secretion and TV increase, but this may reflect their measurement schedule. Whereas they measured T monthly, TV was measured only four times a year (April, July, October, and January). The time lag between TV increase and T secretion in immature individuals is quite different from that between the frequency of breeding behaviors (mounts) and T secretion (Rostal et al. 1986).

The presence of cycling females has been reported to influence males sharing the same environment (Vandenbergh 1969). We found that males in the same cage tended to show similar profiles, and, notably, cycling females were also reared in these cages. We could not, however, substantiate any such influence in this study (see pp 389–392 in Dixson 1998).

Development and seasonality in the nipple size of Japanese macaques

Nipple size variation in macaques has not attracted much attention, though there are studies that deal with nipple preference (laterality, e.g. Tanaka 1989). The size varies widely among individuals because there are many factors influencing it: growth, reproductive maturation, menstrual cycle, physical factors such as suckling by offspring, pregnancy and parturition, lactation, and aging. In the peri-adolescent period, the age change in nipple size appears consistent.

The nipple in Japanese macaques starts to grow rapidly at about 3.5 years of age, in conjunction with other characters that advertise reproductive state (the swelling of sexual skin and reddening of the face and sexual skin). The Japanese macaque subjects showed substantial P secretion in their fourth winter (ca. 3.5 years of age), indicating that they may have commenced their menstruation cycles, and their NV increased accordingly over the fourth summer and autumn. Therefore, it seems that many of them experienced menarche in the autumn and, a few months later, their first ovulation. In the case of rhesus macaques (Terasawa et al. 1983), the period between menarche (30.7 ± 1.2 SE months of age) and first ovulation (48.1 ± 2.2 SE months of age) is much longer than that in Japanese macaques.

The nipples finally mature at around 7 years of age in Japanese macaques (5–10 years, the latter half of adolescence and the young-adult period). Seasonality in NV was evident in every female analyzed longitudinally where there was a peak in the breeding season (winter) and a trough in the delivery season (spring). In contrast to the testis, seasonality in NV, starting from puberty, was not evident in the cross-sectional data analysis because of wide individual variation. Throughout the adult period, from 10 to 25 years of age, NV seems to be consistent, though there may be seasonal fluctuation and a cumulative effect of being suckled by offspring in adult macaques, but these are topics for future study. In general, NV gradually decreases from 25 years of age, when, on average, the post-menopausal period begins (Takahata et al. 1995; Pavelka and Fedigan 1999).

The NV in many individuals correlates strongly with changes in reproductive physiology as represented by the P concentration profile in this study. Thus the NV follows the menstrual cycle, and its peak precedes the P peak by about 2 weeks (the mid-follicular phase). The menstrual cycle is often characterized by the concentration profiles of E2, gonadotropins (LH and FSH), and P (Dixson 1998), and the fact that the NV peak is found in the mid-follicular phase indicates that E2 is the major hormone influencing nipple enlargement. A close relationship has been reported between the E2 level and nipple size in rhesus macaques (Terasawa et al. 1983). Nevertheless, there also exists the possibility that other hormones are also involved.

The combination effect of P and E2 on nipples is worth considering even though Terasawa et al. (1983) found no relationship between P and NV before ovulation in the peri-pubertal phase. In the luteal phase P is secreted mainly in preparation for pregnancy (e.g. synthesis of secretory material by uterine glands, Johnson and Everitt 1995; cellular differentiation in the uterus, Baulieu 1992), and both E2 and P are considered to function in maintaining the increase of NV. In the breeding season, when several menstrual cycles occur, the average NV remains higher than that in the non-breeding season. This difference may be due to the fact that the regular secretion of many hormones, including E2 and P, keeps the nipples large throughout the breeding season. The combination effect of P and E2 is also found in the change of NV during pregnancy. After conception, both P and E2 are secreted and the change in NV parallels the concentration profile of P. It is known that P is an antagonist of mineralocorticoids, causing water retention (Felig et al. 1995). The two hormones, E2 and P, in conjunction with others, influence the breasts of women in the luteal phase (Johnson and Everitt 1995), so their combined effect may influence the nipples in Japanese macaques.

The other pattern of NV change that must be explained is that NV increased in some subjects in the

non-breeding season, from spring to autumn. We suspected that a non-ovulatory menstrual cycle caused this increase. Such cycles have been reported for subjects reared in indoor cages with a relatively high frequency (Nozaki 1991). However, as the subjects for the present study were reared in a cage with an outdoor enclosure, it seems an unlikely explanation. Mori et al. (1997) reported on food-enhanced perineal swelling in Japanese macaques in poor nutritional condition, but, although reproductive state is known to relate closely to nutritional condition (Nigi et al. 1995; Nigi and Morimitsu 1997), it could not be used as an explanation in this case. This, then, is also a subject for future study.

The relationship between NV change and social life

It is widely known that Japanese macaques have a multimale, multi-female type of society and will not make "fission and fusion" as chimpanzees do (e.g. Melnick and Pearl 1987), and they are always attentive to the behavior of other members, such as posture and all kinds of facial and tail movements, however slight. It follows then, that they probably also recognize morphological changes in other individuals. The morphological changes related to reproduction, such as sexual swelling, reddening of the facial and sexual skins, and enlargement of testes and nipples, would function as visual cues. Although NV varies considerably among individuals, the present study showed that changes in a given individual due to seasonality and the menstrual cycle are great enough to be detected by other troop members. Humans familiar with subject macaques can also detect the change. Japanese macaques tend to sit keeping their torsos erect, and this posture ensures that the nipples are visible to other members. Nipples appear to advertise secondarily the reproductive state of an individual, together with the remarkable advertisement found in the anogenital region and the caudal aspects of the thigh that are obscured when the individual sits. The present study suggests that peak NV occurs in the midfollicular phase, that is, about 1 week earlier than ovulation. This pattern is similar to that of the sexual swelling in chacma baboons (Bielert 1986), where the skin swells in the follicular phase and starts to break down around the day of ovulation, and frequent ejaculate is observed around the late follicular phase. As Japanese macaques have keen vision, and reddish nipples contrast sharply against their whitish chest, other troop members can detect the nipple change and respond appropriately.

Nipple size has often been used by human observers to classify adult females as either parous or nulliparous for the determination of population structure with considerable accuracy (H. Ohsawa, personal communications). It is also possible for human observers to determine whether the individual is lactating or not simply by observing the nipples. It is, therefore, thought that macaques can also discriminate that difference. We have yet, however, to elucidate the exact relationship between size changes in nipples and behavioral changes in other individuals.

Acknowledgements We thank the staff of the section of Morphology and the Center for Human Evolution Modeling Research of the Primate Research Institute, Kyoto University, for their help and valuable suggestions. This research was supported by a grant-in-aid for COE Research 2001, a grant-in-aid for Specially Promoted Research (COE) 2002, and grants-in-aid nos. 11833008, 11304059, and 14204083 from the Ministry of Education, Culture, Sports, Science and Technology.

References

Baulieu E-E (1992) Hormones: from molecules to disease. Chapman and Hall, New York

Bielert C (1986) Sexual interactions between captive adult male and female Chacma baboons (*Papio ursinus*) as related to the female's menstrual cycle. J Zool (Lond) 209:521–536

Dixson AF (1998) Primate sexuality. Oxford University Press, Oxford

Felig P, Baxter JD, Frohman LA (1995) Endocrinology and metabolism, 3rd edn. McGraw-Hill, New York

Glick BB (1979) Testicular size, testosterone level, and body weight in male *Macaca radiata*. Folia Primatol 32:268–289

Hamada Y, Hayakawa S, Suzuki J, Ohkura S (1999) Adolescent growth and development in Japanese macaques (*Macaca fuscata*): punctuated adolescent growth spurt by season. Primates 40:439–452

Hamada Y, Hayakawa S, Suzuki J, Watanabe K, Ohkura S (2003) Body fat and its seasonality in Japanese macaques (*Macaca fuscata*). Mamm Study 28:79–88

Hamada Y, Iwamoto M, Watanabe T (1986) Somatometrical features of Japanese monkeys in the Koshima Islet: in viewpoint of somatometry, growth, and sexual maturation. Primates 27:471–484

Hamada Y, Watanabe T, Iwamoto M (1996) Physique Index for Japanese macaques (*Macaca fuscata*): age change and regional variation. Anthropol Sci 104:305–323

Hazama N (1964) Weighing wild Japanese monkeys in Arashiyama. Primates 5(3–4):81–104

Johnson MH, Everitt BJ (1995) Essential reproduction, 4th edn. Blackwell, Oxford

Knobil E, Hotchkiss J (1988) The menstrual cycle and its neuroendocrine control. In: Knobil E, Neill J (eds) The physiology of reproduction, vol 2. Raven, New York, pp 1971–1994

Malina RM, Bouchard C (1991) Growth, maturation, and physical activity. Human Kinetics, Champaign, Ill.

Marson J, Meuris S, Cooper RW, Jouannet P (1991) Puberty in the male chimpanzee: progressive maturation of semen characteristics. Biol Reprod 44:448–455

Mastroianni L, Coutifaris C (1990) Reproductive physiology. In: Rosenfield A, Fathalla MF (eds) The FIGO manual of human reproduction, vol 1. Parthenon, New Jersey

Matsubayashi K, Enomoto T (1983) Longitudinal studies on annual changes in plasma testosterone, body weight and spermatogenesis in adult Japanese monkeys (*Macaca fuscata fuscata*) under laboratory conditions. Primates 24:521–529

Matsubayashi K, Mochizuki K (1982) Growth of male reproductive organs with observation of their seasonal morphlogic changes in the Japanese monkey (*Macaca fuscata*). Jpn J Vet Sci 44:891–902

Melnick DJ, Pearl MC (1987) Cercopithecines in multimale groups: genetic diversity and population structure. In: Smuts BB, Cheney DL, Seyfarth RM, Wranghan RW, Struhsaker TT (eds) Primates societies. University of Chicago Press, Chicago, pp 121–134

Meussy-Dessolle N, Dang DC (1985) Plasma concentration of testosterone, dihydrotestosterone, Δ4-androstenediore, dehydroepiandrosterone and oestradiol-17β in the crab-eating monkeys (*Macaca fascicularis*) from birth to adulthood. J Reprod Fertil 74:347–359

Mori A, Yamguchi N, Watanabe K, Shimizu K (1997) Sexual maturation of female Japanese macaques under poor nutritional conditions and food-enhanced perineal swelling in the Koshima Troop. Int J Primatol 18:553–579

Nigi H, Morimitsu Y, Hayama S (1995) Correlation between pregnancies and fats accumulated in great omentum in the free-ranging Japanese monkeys (in Japanese). Primate 11:291

Nigi H, Morimitsu Y (1997) Correlation between reproductive success and fats accumulated in greater omemtum in the free-ranging female Japanese monkeys at Takasakiyama (in Japanese). Primate Res 13:236

Nigi H, Tiba T, Yamamoto S, Floescheim Y, Ohsawa N (1980) Sexual maturation and seasonal changes in reproductive phenomena of male Japanese monkeys (*Macaca fuscata*) at Takasakiyama. Primates 21:230–240

Nozaki M (1991) Mechanisms controlling seasonal breeding in Japanese monkeys (in Japanese with English abstract). Primate Res 7:103–125

Nozaki M (1994) Mechanisms controlling the seasonal breeding of Japanese monkeys (in Japanese with English abstract). J Reprod Dev 40(6):j105–j115

Pavelka MSM, Fedigan LM (1999) Reproductive termination in female Japanese monkeys: a comparative life history perspective. Am J Phys Anthropol 109:455–464

Primate Research Institute (2003) Guide for the care and use of laboratory primates. Primate Research Institute, Kyoto University http://www.pri.kyoto-u.ac.jp/index.html

Rostal DC, Glick BB, Eaton GG, Resko JA (1986) Seasonality of adult male Japanese macaques (*Macaca fuscata*): androgens and behavior in a confined troop. Horm Behav 20:452–462

Sade DS (1964) Seasonal cycle in size of testes of free-ranging *Macaca mulatta*. Folia Primatol 2:171–180

Suzuki J, Ohkura S, Hayakawa S, Hamada Y (2000) Time series analysis of plasma insulin-like growth factor-I and gonadal steroids in adolescent Japanese macaques (*Macaca fuscata*). J Reprod Dev 46:157–166

Takahata Y, Koyama N, Suzuki S (1995) Do the old aged females experience a long post-reproductive life span? The cases of Japanese macaques and chimpanzees. Primates 36:169–180

Tanaka I (1989) Change of nipple preference between successive offspring in Japanese macaques. Am J Primatol 18:321–325

Tanner JM (1962) Growth at adolescence, 2nd edn. Blackwell, Oxford

Terasawa E, Nass TE, Yeoman RR, Loose MD, Schultz NJ (1983) Hypothalamic control of puberty in the female rhesus macaque. In: Norman RL (ed) Neuroendocrine aspects of reproduction: ORPRC symposia on primate reproduction bilogy. Academic, New York, pp 149–182

Vandenbergh JG (1969) Endocrine coordination in monkeys: male sexual responses to the female. Physiol Behav 4:261–264

Cell Death and Differentiation (2005) 12, 1134–1140

www.nature.com/cdd

Opening of plasma membrane voltage-dependent anion channels (VDAC) precedes caspase activation in neuronal apoptosis induced by toxic stimuli

F Elinder*,[1], N Akanda[1,2,4], R Tofighi[2,4], S Shimizu[3], Y Tsujimoto[3], S Orrenius[2] and S Ceccatelli[2]

[1] Department of Biomedicine and Surgery, Division of Cell Biology, Linköpings Universitet, Linköping SE-581 85, Sweden;
[2] Institute of Environmental Medicine, Division of Toxicology and Neurotoxicology, Karolinska Institutet, Stockholm SE-171 77, Sweden;
[3] Laboratory of Molecular Genetics, Osaka University Medical School and Graduate School of Medicine, 2-2 Yamadaoka, Suita, Osaka 565-0871, Japan
[4] These authors contributed equally to this work
* Corresponding author: F Elinder, Department of Biomedicine and Surgery, Division of Cell Biology, Linköpings Universitet, Linköping SE-581 85, Sweden. Tel: +46-13-22-89-45; Fax: +46-13-22-31-92; E-mail: fredrik.elinder@ibk.liu.se

Received 22.12.04; revised 21.3.05; accepted 21.3.05; published online 29.4.05
Edited by G Melino

Abstract

Apoptotic cell death is an essential process in the development of the central nervous system and in the pathogenesis of its degenerative diseases. Efflux of K^+ and Cl^- ions leads to the shrinkage of the apoptotic cell and facilitates the activation of caspases. Here, we present electrophysiological and immunocytochemical evidences for the activation of a voltage-dependent anion channel (VDAC) in the plasma membrane of neurons undergoing apoptosis. Anti-VDAC antibodies blocked the channel and inhibited the apoptotic process. In nonapoptotic cells, plasma membrane VDAC1 protein can function as a NADH (-ferricyanide) reductase. Opening of VDAC channels in apoptotic cells was associated with an increase in this activity, which was partly blocked by VDAC antibodies. Hence, it appears that there might be a dual role for this protein in the plasma membrane: (1) maintenance of redox homeostasis in normal cells and (2) promotion of anion efflux in apoptotic cells.

Cell Death and Differentiation (2005) **12,** 1134–1140.
doi:10.1038/sj.cdd.4401646; published online 29 April 2005

Keywords: apoptosis; VDAC; patch clamp

Abbreviations: VDAC, voltage-dependent anion channel; STS, staurosporine; PS, phosphatidylserine

Introduction

Apoptotic cell death is an essential process in the development of the central nervous system as well as in the pathogenesis of its degenerative diseases.[1] An early morphological alteration occurring during apoptosis is cell shrinkage, which is associated with an increased cellular efflux of K^+ and Cl^- ions.[2–8] The reduced intracellular K^+ concentration also facilitates the activation of apoptosis-related proteases – the caspases.[9,10] Conversely, blocking K^+ or Cl^- channels prevents cell shrinkage and cell death.[5–8] While the K^+ efflux depends on an increased number of active K^+ channels in the plasma membrane, less is known about the Cl^- efflux.

Here, we present electrophysiological evidence for the activation of the voltage-dependent anion channel (VDAC) in the plasma membrane of neuronal cells undergoing apoptosis. VDAC is normally found in the outer mitochondrial membrane, where it is involved in the early stages of certain forms of apoptotic cell death.[11] We now report that blocking VDAC activation in the plasma membrane of neural cell lines inhibits the apoptotic process, suggesting a critical role of this channel during the early stages of neuronal apoptosis.

Results and Discussion

To study electrophysiological changes during apoptosis, we investigated the mouse hippocampal cell line HT22 and the human neuroblastoma cell line SK-N-MC with the patch-clamp technique. Both cell lines displayed low electrical activity under control conditions in isolated membrane patches as well as in whole-cell recordings. The most prominent current was a K^+ current of delayed-rectifier type (see below). Cell death was induced by the application of 1 μM staurosporine (STS) for 2 h. Exposed cells exhibited typical apoptotic morphology (cf. Figure 1a with b) with nuclear condensation (Figure 1c) and exposure of phosphatidylserine (PS) on the cell surface (Figure 1d). In addition, at this time point (2 h), there was an apparent release of cytochrome *c* from the mitochondria (Figure 1e), but yet no caspase activation (data not shown). In accordance with a previous report,[5] we found an apoptosis-associated increase in a K^+ current of delayed-rectifier type. In whole-cell patch-clamp recordings of HT22 cells, the current was activated by voltage steps more positive than −20 mV, and the K^+ channel blocker tetraethylammonium (TEA) at 10 mM reduced the current by 60% (data not shown). Recordings 3–4 min after whole-cell formation showed a dramatic increase in the K^+ current for apoptotic cells in comparison to control cells (+180%, $P<0.05$; Wilcoxon's rank sum test, $n=37$).

VDAC is activated during apoptosis

While ion channel currents were relatively infrequent in membrane patches from control cells, a large-conductance ion channel current was frequently seen in apoptotic cells. Hence, in 10% of cell-attached recordings of apoptotic HT22 cells, we observed large square-like single-channel currents (Figure 2a). Excision of the membrane patch from the cell surface increased the activity of the large-conductance

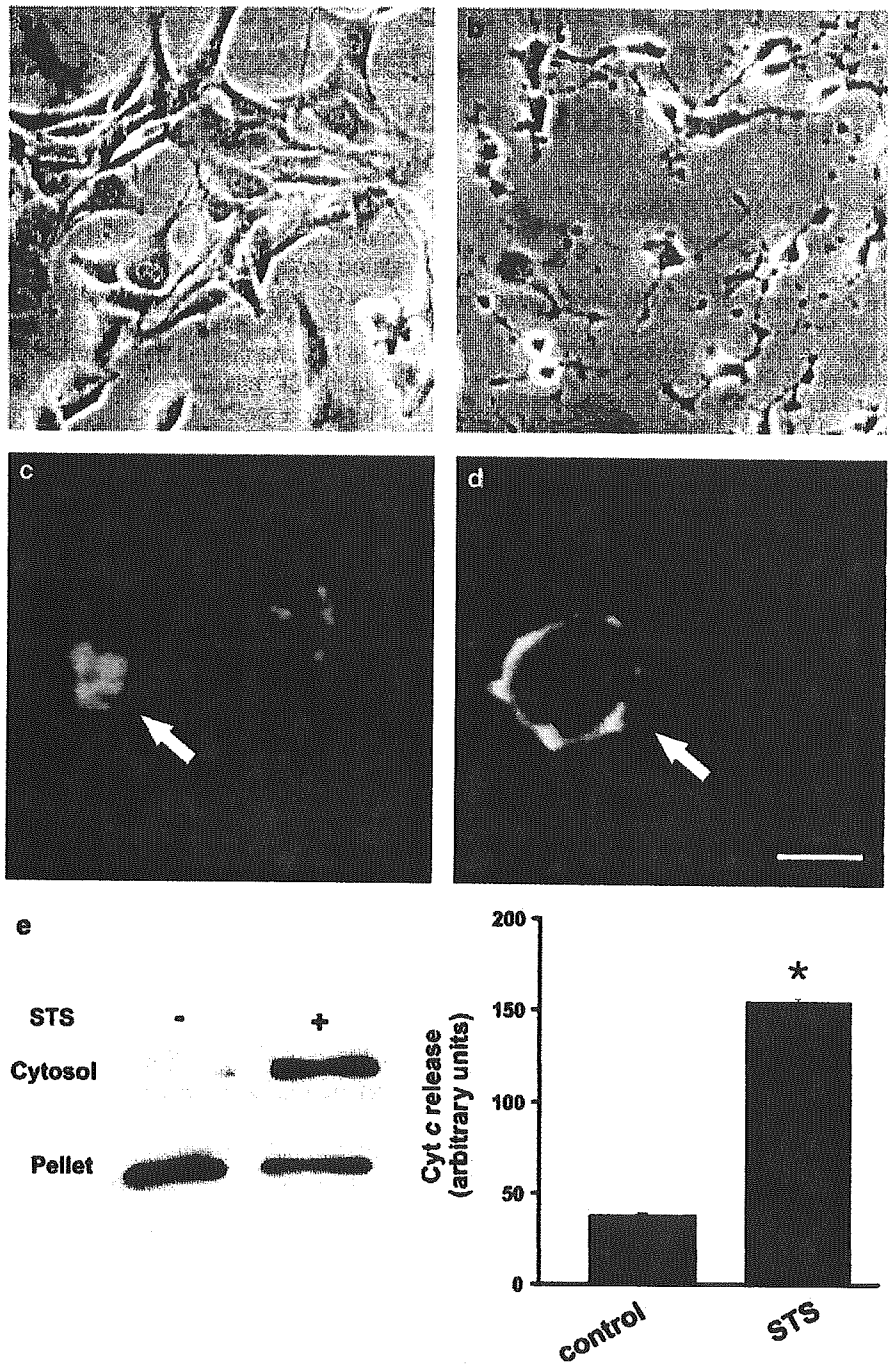

Figure 1 STS induces morphological changes typical for apoptotic cell death. (**a** and **b**). Phase-contrast micrographs of control (**a**) and exposed (**b**) HT22 cells showing cell shrinkage induced by 1 μM STS for 2 h. (**c** and **d**) Apoptotic cells exhibit nuclear condensation as visualized by staining with Hoechst 33358 (arrow in **c**), and exposure of PS on the outer surface of the plasma membrane, as detected by Annexin V–FITC, a phospholipid-binding protein with high affinity for PS (arrow in **d**). Scale bar = 70 μm in (**a** and **b**), and 15 μm in (**c** and **d**). (**e**) Immunoblot showing cytochrome *c* release from the mitochondria to the cytosol in cells exposed to STS. The quantification of cytosolic cytochrome *c* was performed by measurement of band density on film after immunoblotting. Values are means $\pm$ S.E.M. of three determinations. Statistical analysis was performed with the two-tailed Student's *t*-test (*$P<0.001$)

channel with a time constant of about 2 min (Figure 2b). The large-conductance channel was found in 48% of the excised inside-out membrane patches from apoptotic cells (24/50), but only occasionally in similar patches from control cells (2/50) (χ^2-test $P<0.01$; Figure 2c). Up to six channels were found in a single-membrane patch. The channel was voltage dependent with an open probability around 70% at 0 mV, which was drastically decreased at both positive and negative voltages (Figure 2d and e). The single-channel conductance was 397 pS, and the reversal potential was 0 mV (Figure 2f). The same large-conductance channel was also seen when apoptosis was induced by 2,3-dimethoxy-1,4-naphthoqui-

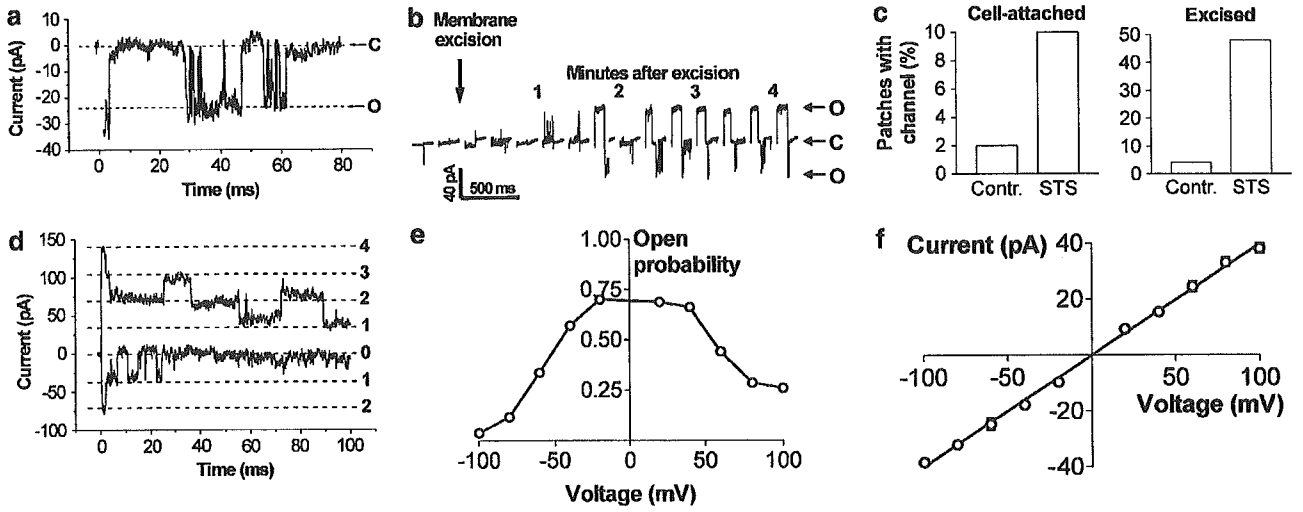

Figure 2 Electrophysiological properties of a large-conductance channel in the plasma membrane of (STS-induced) apoptotic HT22 cells. (**a**) Large-conductance channel in cell-attached mode. Holding voltage (V_H, defined as bath voltage−pipette voltage) is 0 mV and test step voltage is −80 mV. Extracellular solution in the pipette and the bath. C and O denotes closed and open states. (**b**) Consecutive recordings every 20 s. $V_H = 0$ mV is followed by 100 ms at + 100 mV and 100 ms at −100 mV in each recording. The large-conductance channel is clearly conducting about 2 min after excision of the membrane patch. (**c**) Frequency diagram of large-conductance channels in cell-attached and -excised inside-out patches for control and (STS-induced) apoptotic cells. (**d**) Several channels in a patch. Upper current for a voltage-clamp step to + 100 mV from $V_H = 0$ mV. Lower current for a step to −100 mV. The dashed lines are separated with 37 pA. The figures denote the number of open channels. (**e**) Open probability after 100 ms at the indicated voltages. $V_H = 0$ mV. Data from three consecutive recordings with channels in 10 patches ($n = 30$). (**f**) *I*(*V*) plot for single-channel current in inside-out membrane patches. Conductance is 397 ± 12 pS and the reversal potential is −0.2 ± 2.0 mV ($n = 6$). S.E.M. bars are hidden by the symbols

none, methyl mercury, or styrene 7,8-oxide in both HT22 and SK-N-MC cells (data not shown).

Thus, there was a much higher channel activity in apoptotic cells compared to control cells in both cell-attached and excised membrane patches (Figure 2c). In addition, this activity increased dramatically when the membrane patch was excised from the intact cell. To investigate the mechanism responsible for this increase in activity, we performed patch-clamp experiments in which the intracellular side of excised inside-out patches was perfused with intracellular solutions with or without either 4 mM ATP, 100 μM cAMP, or 500 μM Ca^{2+}. ATP reversibly blocked the channel activity, while cAMP and Ca^{2+} had no effect (data not shown). Thus, loss of ATP could possibly contribute to the increase in activity in intact apoptotic cells. To test this hypothesis, we measured ATP levels in HT22 cells exposed to STS for 2 h and found a significant decrease of 38% in cells undergoing apoptosis as compared to control cells. This drop in ATP level is compatible with apoptotic cell death.[12]

To identify the channel, we characterized its ion selectivity and pharmacological properties. Taken together, our findings are compatible with a VDAC. Changing from an extracellular (mainly NaCl) to an intracellular (mainly KCl) solution in the bath did not affect the current in inside-out membrane patches (data not shown), suggesting that the channel does not select between Na^+ and K^+ ions. Dilution of the bath solution to 1/5 of its original concentration decreased the current from the (extracellular) pipette solution to the (intracellular) bath solution dramatically, while leaving the current in the opposite direction essentially unchanged (Figure 3a). The reversal potential was shifted from 0 to −41 ± 6 mV (Figure 3b). A cation channel (no Cl^- permeability) predicts a shift of + 41 mV, a nonselective channel predicts no shift, while a

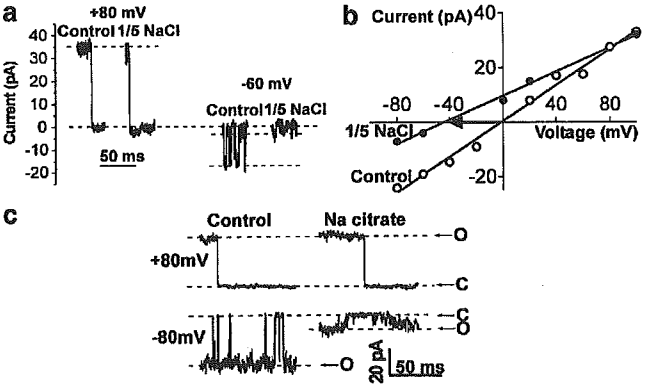

Figure 3 Selectivity and pharmacological properties of a large-conductance channel in the plasma membrane of (STS-induced) apoptotic HT22 cells. (**a**) Diluting the bath solution to 1/5 of its original concentration (intracellular side of the patch) reduces the current at −60 mV, but not at + 80 mV, $V_H = 0$ mV. (**b**) *I*(*V*) plots from control and diluted solutions. Reversal potential is shifted −41 mV, suggesting that the channel is Cl^- selective. (**c**) $Citrate^{3-}$ ions instead of Cl^- ions in the bath solution reduces the current at −80 mV, but not at + 80 mV

Cl^- channel predicts a shift of −41 mV, suggesting that the large-conductance channel is mainly Cl^- selective (see equation 1 in Materials and Methods). To further study the ion permeating pore, we exchanged the Cl^- ion in the bath solution for the much larger trivalent citrate ion. This reduced the current but did not abolish it (Figure 3c), suggesting that the ion-conducting pore must be relatively wide (>7–8 Å). Taken together, the electrophysiological data ((1) large conductance of about 400 pS, (2) bell-shaped open probability curve, and (3) Cl^- selectivity) suggest that the large-conductance channel in the plasma membrane described

here is similar to the VDAC, normally present in the mitochondrial outer membrane.[13]

Although there are certain differences between our observations and the reported properties of VDAC,[13–19] this variability may be ascribed to differences in experimental preparations and conditions. For instance, the difference in the (main state) conductance between cellular preparations and VDACs reconstituted in black lipid bilayer depends on different salt concentrations (140 mM *vs* 1 M). We did not report any small-subconductance state normally seen in VDACs in black lipid bilayer. The reason for this is that these smaller conductances are difficult to separate from other cellular ion channels (e.g. K channels). We also excluded that the activity reported here was due to a volume-sensitive, outwardly rectifying Cl^- channel, which has previously been associated with apoptosis.[20,21] This is based on the following observations: (1) The current channel has a much larger conductance in physiological solutions (400 *vs* 20–80 pS), (2) it has a different voltage dependence of the open probability curve (bell shaped *vs* sigmoidal), and (3) it has the opposite ATP dependence (decrease *vs* increase in activity with increasing ATP concentration).

To further establish the identity between the large-conductance channel and VDAC, we performed experiments with two different anti-VDAC antibodies recognizing different epitopes.[11] Both antibodies showed similar VDAC-like immunoreactivity in the plasma membrane of HT22 cells (Figure 4a and Figure S1 in Supplementary information).

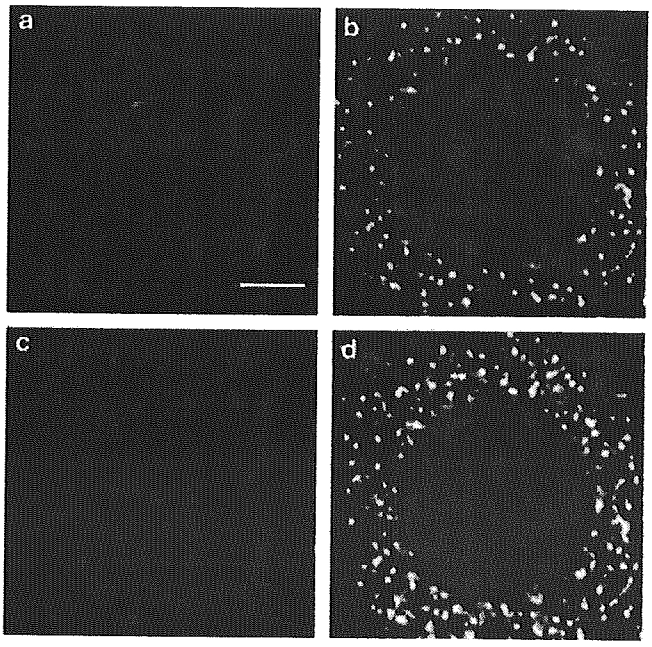

Figure 4 Immunofluorescence micrographs showing VDAC-like immunoreactivity. (**a**) Unfixed control HT22 cells incubated with the anti-VDAC antibody Ab25[11] displays VDAC-like immunoreactivity in the plasma membrane. (**b–d**) To visualize mitochondrial VDAC, cells were incubated with MitoTracker Red for 30 min, then fixed with 4% paraformaldehyde and incubated overnight with anti-VDAC antibody Ab25. The micrographs show a control cell stained with VDAC antibody (**b**) and MitoTracker Red (**c**). Merging of the images in (**b**) and (**c**) demonstrate the mitochondrial localization of VDAC (**d**). Scale bar = 17 μm in (**a**), and 6 μm in (**b–d**)

Using the same antibodies on fixed cells preincubated with MitoTracker Red, we observed dot-like cytoplasmatic VDAC immunoreactivity localized in mitochondria (Figure 4b–d). Plasma membrane VDACs were detected in both control and apoptotic cells, suggesting that the channels are constitutively present in the plasma membrane, but activated only during apoptosis.

Anti-VDAC antibodies block channel activity and prevent apoptosis

The finding of VDAC-like activity in the plasma membrane of apoptotic cells raises questions about its functional role, and whether it is required for the apoptotic process. We investigated this by occluding the channel with different VDAC blockers: (1) We used three anti-VDAC antibodies (Ab25; Ab31; Ab20) recognizing different epitopes.[11] Preincubation of HT22 cells with VDAC antibodies for 30 min prior to exposure to STS blocked plasma membrane VDAC activation (Figure 5a; see also Figure S2a, in Supplementary information) and drastically reduced the number of apoptotic cells, as detected by nuclear condensation (Figure 5b; see also Figure S2b in Supplementary information) or PS exposure (not shown). In contrast, an unrelated antibody (Neurofilament) did not prevent VDAC activity (data not shown). (2) The addition of 240 mM sucrose to the diluted 1/5 solution described above and in Materials and Methods was found to block the single-channel current by 90% (Figure 5c), without affecting the reversal potential. In line with the hypothesis that blocking plasma membrane VDACs also prevents apoptosis, we found a significant decrease in the number of apoptotic cells induced by STS, when they had been preincubated with sucrose (Figure 5d). Most likely, the antiapoptotic effect of sucrose was not influenced by the low Cl^- concentration in the medium, which would be expected to increase the Cl^- efflux rather than decrease it. Hence, functional VDACs in the plasma membrane are induced by triggers of apoptosis. Blocking these channels prevents apoptosis, suggesting an essential role for plasma membrane VDAC in apoptotic cell death.

Functional expression of plasma membrane VDACs in apoptotic cells seems to occur concomitant with cytochrome *c* release, but upstream of caspase activation. To ascertain this, we also performed electrophysiological experiments in which cells were exposed to the global caspase inhibitor zVAD-fmk prior to STS. As expected, pretreatment with the caspase inhibitor did not prevent STS-induced VDAC currents (data not shown).

VDAC in the plasma membrane

VDAC was originally detected in the outer mitochondrial membrane, where it mediates the translocation of various metabolites and other compounds in and out of the mitochondria (e.g. pyruvate, malate, ADP, ATP, etc). It has also been found to be an important player in the regulation of mitochondrial cytochrome *c* release in some forms of apoptosis by interacting with members of the Bcl-2 family of proteins.[22,23] Further, VDAC is one of the components of the

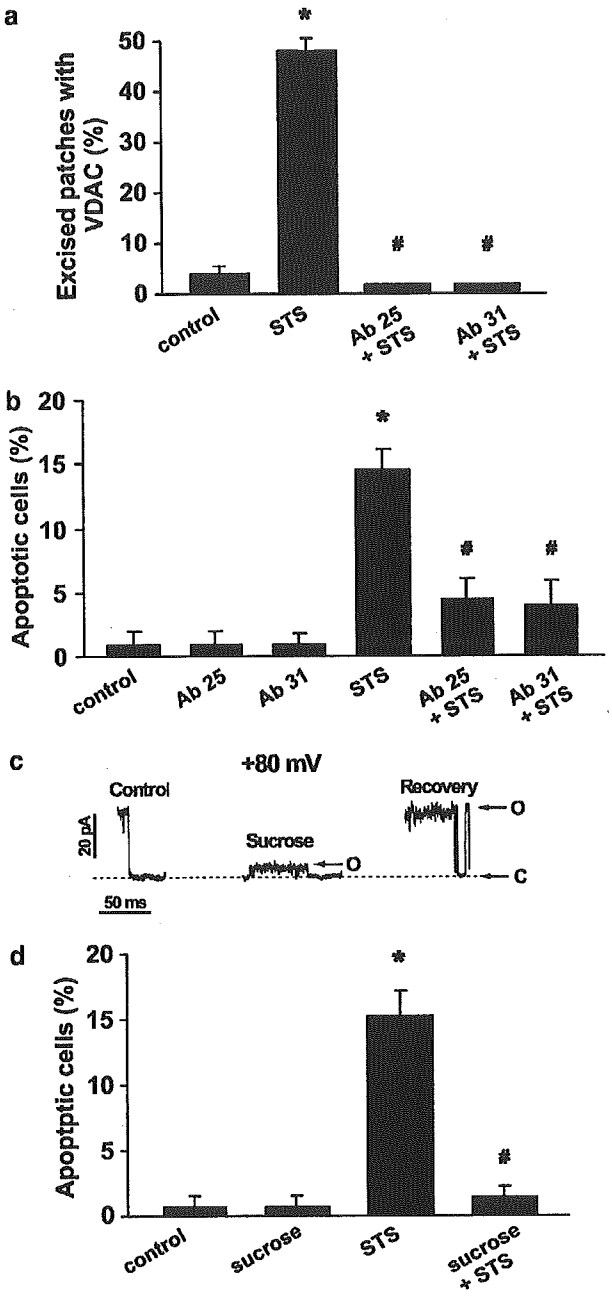

Figure 5 Blocking of plasma membrane VDAC prevents apoptosis. (**a** and **b**) Preincubation of HT22 cells with different VDAC antibodies (Ab25 or Ab31) for 30 min prior to exposure to STS-blocked plasma membrane VDAC activation (**a**) and drastically reduced the occurrence of cell death (**b**). (**c**) Sucrose (240 mM) added to the diluted (1/5) solution clearly reduce the current at +80 mV. (**d**) Sucrose also prevented induction of apoptosis by STS as evaluated by the vital triple staining with PI, Hoechst 33358, and Annexin V. Statistical analysis was performed with ANOVA (Fisher's PLSD test). *Significantly different from control or sucrose; #Significantly different from STS ($P<0.0001$)

mitochondrial permeability transition pore complex, which has also been implicated in the release of cytochrome *c* leading to caspase activation and apoptosis.[24]

The presence of VDAC in the plasma membrane has been debated.[25] However, several reports, using different techniques, have shown VDAC-like channels in the plasma membrane of multiple cell types, including neurons.[14–16,26–28] A major argument against the presence of functional VDACs in the plasma membrane has been that this would result in increased membrane permeability that would not be compatible with cell survival. Therefore, as suggested by Yu and Forte,[25] it is likely that these channels are not functional under normal conditions. Our data support this hypothesis, while pointing to a critical role for plasma membrane VDAC in apoptotic cell death.

Recently, it has been demonstrated that the VDAC1 protein in the plasma membrane can function as an NADH (-ferricyanide) reductase previously proposed to be involved in transmembranous redox regulation.[27] This finding together with the current demonstration of the appearance of VDAC electrophysiological activity in apoptotic cells suggests a dual role for the plasma membrane VDAC1 protein, that is, maintenance of cellular redox homeostasis in normal cells and cell volume regulation in apoptotic cells. To further investigate this hypothesis, we measured NADH (-ferricyanide) reductase activity in intact control and STS-treated HT22 cells. Cells exposed to 1 μM STS showed a time-dependent increase in NADH (-ferricyanide) reductase activity (Figure 6a). Like the appearance of VDAC electrophysiological activity in apoptotic cells, stimulation of the

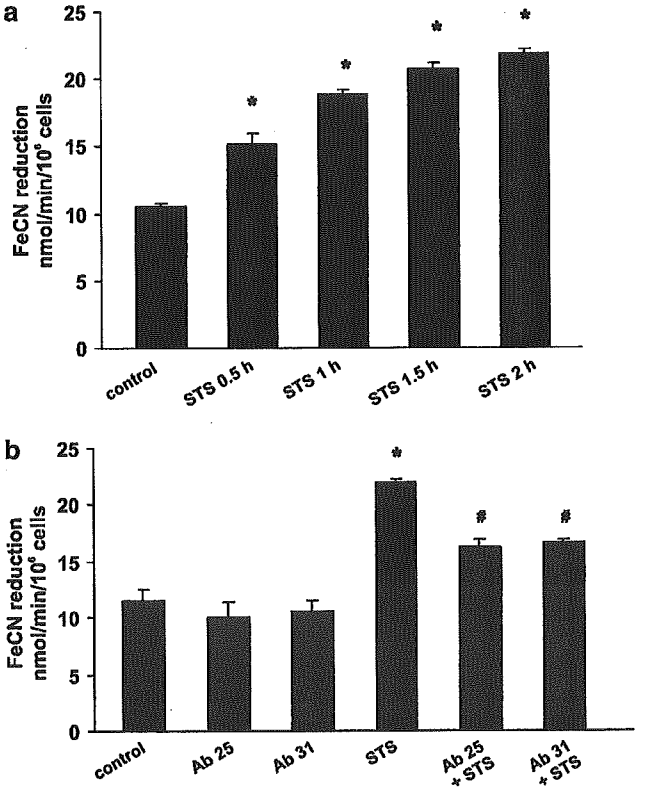

Figure 6 Stimulation of NADH (-ferricyanide) reducatse activity in apoptotic cells and its partial inhibition by anti-VDAC antibodies. (**a**) HT22 cells exposed to 1 μM STS showed a time-dependent increase in NADH (-ferricyanide) reductase activity. (**b**) Preincubation of the cells with anti-VDAC antibodies Ab25 or Ab31 partly prevented the STS-induced increase in NADH (-ferricyanide) reductase activity. Statistical analysis was performed with ANOVA (Fisher's PLSD test). *Significantly different from control or Ab25 or Ab31; #Significantly different from STS ($P<0.0001$)

reductase activity was inhibited by treatment of the cells with anti-VDAC antibodies prior to exposure to STS (Figure 6b). The unrelated antibody Neurofilament did not inhibit the reductace activity. Hence, it appears that both the electrophysiological and NADH (-ferricyanide) reductase activities of the VDAC protein are stimulated in apoptotic cells, and that this stimulation is inhibited by anti-VDAC antibodies.

In summary, we have shown that the expression of functional VDAC activity is induced by a number of apoptotic stimuli in the plasma membrane of two neuronal cell lines, and that blocking this activity prevents apoptosis. The activation of VDAC appears to be concomitant with mitochondrial cytochrome *c* release and the opening of K^+ channels, but upstream caspase activation. The conjunction of open Cl^- and K^+ channels leads to Cl^- and K^+ efflux, cell shrinkage, and further activation of the apoptotic process. In both control and apoptotic cells, the VDAC protein can function as an NADH (-ferricyanide) reductase. How this is regulated, and how the electrophysiological activity of the protein is triggered in apoptotic cells, are subject to current investigation in our laboratories.

Materials and Methods

Cell culture and treatment

Cells (HT22 and SK-N-MC) were incubated in CO_2-independent medium (Gibco BRL, Stockholm, Sweden, 18045-054) containing 10% fetal calf serum, 4 mM L-glutamine, 100 U/ml penicillin, and 100 μg/ml streptomycin. Cells were incubated at 100% relative humidity and at 37°C for 24 h before exposure to the apoptotic stimuli. All chemicals for cell culture were supplied by Life Technologies (Gibco BRL). To induce apoptosis, cells were exposed to 1 μM STS,[29] 30 μM 2,3-dimethoxy-1,4-naphthoquinone, 4 μM methylmercury, or 0.3 mM styrene 7,8-oxide,[30] for 1.5–6.5 h. To prevent apoptosis, cells were preincubated with anti-VDAC antibodies Ab25[11] (1 : 200), antibodies Ab20[11] (1 : 200), anti-Porin 31 HL Ab-2 (Ab31) (Calbiochem)[11] (1 : 100), or the pancaspase inhibitor zVAD-fmk (20 μM). As a negative control, we used an unrelated antibody Neurofilament (DSHB, IA, USA). In some experiments, cells were preincubated with sucrose (240 mM).

Electrophysiology

The electrophysiological recordings were carried out with the patch-clamp technique. We used an EPC-7 patch-clamp amplifier (List Instruments) and pClamp software (Axon Instruments). The extracellular solution was composed of (in mM): 140 NaCl, 5 KCl, 1.8 $CaCl_2$, 1 $MgCl_2$, 10 HEPES, and 23 sucrose (pH 7.4). The intracellular solution was composed of (in mM): 4 NaCl, 140 KCl, 0.5 $CaCl_2$, 1 $MgCl_2$, 10 HEPES, and 5 EGTA (pH 7.4). For the recordings with the citrate ions, instead of using 140 mM NaCl, we used 46.7 mM $(Na)_3$citrate supplemented with 93.3 mM sucrose to retain the osmolarity. The patch pipettes were made of borosilicate glass and the pipette resistance was 4–6 MΩ with the solutions used. In cell-attached and inside-out recordings, the pipettes were filled with the extracellular solution. In the whole-cell recordings, the pipettes were filled with the intracellular solution. In cell-attached and whole-cell recordings, the extracellular solution was used in the bath. In the inside-out recordings presented in the paper, we used the intracellular solution in the bath. We also tried the extracellular solution on the intracellular side of inside-out patches. No difference was seen regarding VDAC activity. The current was always denoted as positive for currents from the intracellular side toward the extracellular pipette side. Leakage current and capacitive currents were removed by subtraction of corresponding traces with no channel activity. For the analysis of the shift of the reversal potential (ΔV_{rev}), we used the following equation:

$$\Delta V_{rev} = -RT/Fz \ln([X]_{test}/[X]_{control}) \quad (1)$$

where R, T, and F have their normal thermodynamic significances, z is the valence of the ion X, and $[X]$ is the concentrations of the ion X in different solutions.

Evaluation of apoptotic cells

The occurrence of apoptosis was evaluated on fixed or living cells. Cells grown on coverslips were fixed with ice-cold methanol/water (8/2 = v/v), and stained with cell-impermeable propidium iodide (PI) to visualize nuclear condensation. Apoptotic cells were identified by the smaller size of the nucleus, irregular shape, and brighter intensity of the stained chromatin. For vital stainings, cells grown on coverslips were incubated with a solution of Annexin V–FITC (0.5 μg/ml), which binds to PS, PI (1 μg/ml), and cell-permeable Hoechst 33358 (1 μg/ml) in a buffer containing 10 mM HEPES/NaOH (pH 7.4), 140 mM NaCl, and 2.5 mM $CaCl_2$. Cells were analyzed with an Olympus BX60 fluorescence microscope equipped with a Hamamatsu digital camera ORCA II.

Immunoblotting and immunocytochemistry

To monitor the release of mitochondrial cytochrome *c* into the cytosol, the cytosolic fractions from control and exposed cells were separated from the mitochondria.[31] Cytochrome *c* was detected by immunoblotting with a primary mouse antibody (1 : 2500, BD-Pharmingen, San Diego, CA, USA) and with a goat anti-mouse secondary antibody, horseradish peroxidase-conjugated (dilution 1 : 20 000, Pierce Rockford, IL, USA), according to methods described previously.[31] Immunoblot bands were quantified with an LKB Ultrascan XL laser densitometer. Immunocytochemistry was performed on unfixed or fixed (4% paraformaldehyde) cells. In order to prevent endocytosis of any added antibodies, living cells were blocked with BSA–PBS for 5 min at 4°C. Fixed or unfixed cells were then incubated overnight at 4°C with two different anti-VDAC antibodies, one raised in rabbit (Ab25[11]) (1 : 200), and the other one in mouse (anti-Porin 31 HL Ab-2) (1 : 100). After several washes with PBS, fluorescein isothiocyanate (FITC)-conjugated goat anti-rabbit or donkey anti-mouse (Jackson) antibodies were added as secondary antibodies for 30 min at 4°C. For control purpose, cells were also incubated with the secondary antibodies alone. In some experiments, living cells were preincubated with the MitoTracker Red (100 nM) (Molecular Probes) for 30 min, fixed and stained as above. Stained cells were analyzed with a fluorescence microscope and images captured as described above, or with a confocal microscope BioRad Radiance Plus.

ATP determination

ATP concentrations were determined in a luminometric assay using the ATP dependency of the light-emitting luciferase-catalyzed oxidation of luciferin (Boehringer Mannheim, Mannheim, Germany) according to the manufacturer's protocol. Briefly, cells (5.0×10^5) were resuspended in 50 μl PBS and 450 μl of boiling lysing buffer (100 mM Tris, 4 mM EDTA (pH 7.75)) were added. Samples were incubated for another 2 min at 100°C and 100 μl were taken out to a 96-well plate. Prior to measurement,

100 μl of luciferase were added to each well and the plate was analyzed in a luminometer (Berthold, R-Biopharm AG, Germany).

NADH (-ferricyanide) reductase activity

Cells (4×10^6) were harvested and incubated in 1 ml buffer, containing 50 mM Tris-HCl (pH 8.0) and 250 μM β-NADH for 5 min at 37°C. The reaction was started by the addition of 250 μM potassium ferricyanide to the reaction buffer leading to reduction of ferricyanide to ferrocyanide. After 10 min, cells were spun down and the concentration of remaining ferricyanide was assessed, using a UNICAM 5625 spectrophotometer, at 420 nm. Ferricyanide reductase activity was calculated as nmol ferricyanide reduced per min per 10^6 cells.

Acknowledgements

We thank Peter Larsson (OHSU), Peter Århem (KI), and Roope Männikkö (KI) for comments on this paper; Zhi-Qing David Xu and Vladimir Gogvadze for helping with confocal microscopy and the NADH reductase assay, respectively. This study was supported by grants from the Swedish Research Council (FE, SC), European Commission (CT-2003-506143) (SC), Åke Wibergs Stiftelse (FE), and Magnus Bergvalls Stiftelse (FE).

References

1. Heidenreich KA (2003) Molecular mechanisms of neuronal cell death. Ann. NY Acad. Sci. 991: 237–250
2. Barbiero G, Duranti F, Bonelli G, Amenta JS and Baccino FM (1995) Intracellular ionic variations in the apoptotic death of L cells by inhibitors of cell cycle progression. Exp. Cell Res. 217: 408–410
3. Benson RS, Heer S, Dive C and Watson AJ (1996) Characterization of cell volume loss in CEM-C7A cells during dexamethasone-induced apoptosis. Am. J. Physiol. 270: C1190–C1203
4. Bortner CD, Hughes Jr FM and Cidlowski JA (1997) A primary role for K^+ and Na^+ efflux in the activation of apoptosis. J. Biol. Chem. 272: 32436–32442
5. Yu SP, Yeh C-H, Sensi SL, Gwag BJ, Canzoniero LMT, Farhangrazi ZS, Ying HS, Tian M, Dugan LL and Choi DW (1997) Mediation of neuronal apoptosis by enhancement of outward potassium current. Science 278: 114–117
6. Colom LV, Diaz ME, Beers DR, Neely A, Xie WJ and Appel SH (1998) Role of potassium channels in amyloid-induced cell death. J. Neurochem. 70: 1925–1934
7. Wang L, Xu D, Dai W and Lu L (1999) An ultraviolet-activated K^+ channel mediates apoptosis of myeloblastic leukemia cells. J. Biol. Chem. 274: 3678–3685
8. Maeno E, Ishizaki Y, Kanaseki T, Hazama A and Okada Y (2000) Normotonic cell shrinkage because of disordered volume regulation is an early prerequisite to apoptosis. Proc. Natl. Acad. Sci. USA 97: 9487–9492
9. Hughes Jr FM, Bortner CD, Purdy GD and Cidlowski JA (1997) Intracellular K^+ suppresses the activation of apoptosis in lymphocytes. J. Biol. Chem. 272: 30567–30576
10. Cain K, Langlais C, Sun XM, Brown DG and Cohen GM (2001) Physiological concentrations of K^+ inhibit cytochrome *c*-dependent formation of the apoptosome. J. Biol. Chem. 276: 41985–41990
11. Shimizu S, Matsuoka Y, Shinohara Y, Yoneda Y and Tsujimoto Y (2001) Essential role of voltage dependent anion channel in various forms of apoptosis in mammalian cells. J. Cell Biol. 152: 237–250
12. Leist M, Single B, Castoldi A, Kuhnle S and Nicotera P (1997) Intracellular adenosine triphosphate (ATP) concentration: a switch in the decision between apoptosis and necrosis. J. Exp. Med. 185: 1481–1486
13. Columbini M, Blachly-Dyson E and Forte M (1996) VDAC, a channel in the outer mitochondrial membrane In *Ion Channels*, Vol. 4, Narahashi T (ed) (New York: Plenum Press) pp. 169–202
14. Blatz AL and Magleby KL (1983) Single voltage dependent chloride-selective channels of large conductance in cultured rat muscle. Biophys. J. 43: 237–241
15. Jalonen T, Johansson S, Holopainen I, Oja SS and Århem P (1989) A high-conductance multi-state anion channel in cultured rat astrocytes. Acta Physiol. Scand. 136: 611–612
16. Dermietzel R, Hwang TK, Buettner R, Hofer A, Dotzler E, Kremer M, Deutzmann R, Thinnes FP, Fishman GI, Spray DC and Siemen D (1994) Cloning and *in situ* localization of a brain-derived porin that constitutes a large-conductance anion channel in astrocytic plasma membranes. Proc. Natl. Acad. Sci. USA 91: 499–503
17. Guibert B, Dermietzel R and Siemen D (1998) Large conductance channel in plasma membranes of astrocytic cells is functionally related to mitochondrial VDAC-channels. Int. J. Biochem. Cell Biol. 30: 379–391
18. Báthori G, Szabó I, Schmehl I, Tombola F, De Pinto V and Zoratti M (1998) Novel aspects of the electrophysiology of mitochondrial porin. Biochem. Biophys. Res. Comm. 243: 258–263
19. Bahamonde MI, Fernández-Fernández JM, Guix FX, Vázquez E and Valverde MA (2003) Plasma membrane voltage-dependent anion channel mediates antiestrogen-activated maxi Cl^- currents in C1300 neuroblastoma cells. J. Biol. Chem. 278: 33284–33289
20. Okada Y (1997) Volume expansion-sensing outward-rectifier Cl^- channel: fresh start to the molecular identity and volume sensor. Am. J. Physiol. 273: C755–C789
21. Shimizu T, Numata T and Okada Y (2004) A role of reactive oxygen species in apoptotic activation of volume-sensitive Cl^- channel. Proc. Natl. Acad. Sci. USA 101: 6770–6773
22. Shimizu S, Narita M and Tsujimoto Y (1999) Bcl-2 family proteins regulate the release of apoptogenic cytochrome c by the mitochondrial channel VDAC. Nature 399: 483–487
23. Rostovtseva TK, Antonsson B, Suzuki M, Youle RJ, Colombini M and Bezrukov SM (2004) Bid, but not Bax, regulates VDAC channels. J. Biol. Chem. 279: 13575–13583
24. Zheng Y, Shi Y, Tian C, Jiang C, Jin H, Chen J, Almasan A, Tang H and Chen Q (2004) Essential role of the voltage-dependent anion channel (VDAC) in mitochondrial permeability transition pore opening and cytochrome *c* release induced by arsenic trioxide. Oncogene 23: 1239–1247
25. Yu WH and Forte M (1996) Is there VDAC in cell compartments other than the mitochondria? J. Bioenerg. Biomembr. 28: 93–100
26. Thinnes FP and Reymann S (1997) New findings concerning vertebrate porin. Naturwissenschaften 84: 480–498
27. Baker MA, Lane DJR, Ly JD, De Pinto V and Lawen A (2004) VDAC1 is a transplasma membrane NADH-ferricyanide reductase. J. Biol. Chem. 279: 4811–4819
28. Buettner R, Papoutsoglou G, Scemes E, Spray DC and Dermietzel R (2000) Evidence for secretory pathway localization of a voltage-dependent anion channel isoform. Proc. Natl. Acad. Sci. USA 97: 3201–3206
29. Gorman AM, Hirt UA, Orrenius S and Ceccatelli S (2000) Dexamethasone pre-treatment interferes with apoptotic death in glioma cells. Neuroscience 96: 417–425
30. Dare E, Tofighi R, Vettori MV, Momoi T, Poli D, Saido TC, Mutti A and Ceccatelli S (2002) Styrene 7,8-oxide induces caspase activation and regular DNA fragmentation in neuronal cells. Brain Res. 933: 12–22
31. Robertson JD, Enoksson M, Suomela M, Zhivotovsky B and Orrenius S (2002) Caspase-2 acts upstream of mitochondria to promote cytochrome *c* release during etoposide-induced apoptosis. J. Biol. Chem. 277: 29803–29809

Supplementary Information accompanies the paper on Cell Death and Diffrentiation website (http://www.nature.com/cdd)

Available online at www.sciencedirect.com
SCIENCE DIRECT®
Biochemical and Biophysical Research Communications 333 (2005) 427–431
BBRC
www.elsevier.com/locate/ybbrc

Chk2 regulates transcription-independent p53-mediated apoptosis in response to DNA damage ☆

Chen Chen [a], Shigeomi Shimizu [b], Yoshihide Tsujimoto [b], Noboru Motoyama [a,*]

[a] *Department of Geriatric Research, National Institute for Longevity Sciences, National Center for Geriatrics and Gerontology, Obu, Aichi 474-8522, Japan*
[b] *Department of Post-Genomics Diseases, Osaka University Medical School, Suita, Osaka 565-0871, Japan*

Received 17 May 2005
Available online 2 June 2005

Abstract

The tumor suppressor protein p53 plays a central role in the induction of apoptosis in response to genotoxic stress. The protein kinase Chk2 is an important regulator of p53 function in mammalian cells exposed to ionizing radiation (IR). Cells derived from *Chk2*-deficient mice are resistant to the induction of apoptosis by IR, and this resistance has been thought to be a result of the defective transcriptional activation of p53 target genes. It was recently shown, however, that p53 itself and histone H1.2 translocate to mitochondria and thereby induces apoptosis in a transcription-independent manner in response to IR. We have now examined whether Chk2 also regulates the transcription-independent induction of apoptosis by p53 and histone H1.2. The reduced ability of IR to induce p53 stabilization in Chk2-deficient thymocytes was associated with a marked impairment of p53 and histone H1 translocation to mitochondria. These results suggest that Chk2 regulates the transcription-independent mechanism of p53-mediated apoptosis by inducing stabilization of p53 in response to IR.

Keywords: Apoptosis; Chk2; p53; Histone H1; Mitochondria; Thymocytes; Ionizing radiation; Transcription

The genome of cells is continually damaged by environmental insults such as ultraviolet light and ionizing radiation (IR); by oxidative stress, such as that attributable to reactive oxygen species derived from oxidative metabolism; and, in dividing cells, by errors in DNA replication and mitosis. Maintenance of the integrity of genomic DNA relies on the DNA damage checkpoint, which either halts cell cycle progression to allow cells time to repair DNA damage or triggers apoptosis, depending on the extent of DNA damage and on cell type [1–3]. By acting as a central regulator of cell cycle arrest and apoptosis, the tumor suppressor protein p53 protects cells from malignant transformation. This role has earned p53 the designation of "guardian of the genome" or "gatekeeper of the cell" [4,5]. Among the multiple specific functions of p53, the induction of apoptosis is thought to be especially important in preventing tumor progression [6,7].

Regulation of the abundance and transcriptional regulatory activity of p53 is achieved primarily by posttranscriptional modification, including phosphorylation and acetylation [8]. Exposure of cells to IR activates a signaling pathway that includes sensors of DNA damage, signal transducers, and mediators and which results in the stabilization and activation of p53 [1–3]. We and others have previously shown that Chk2 contributes to p53 stabilization in cells exposed to IR and that Chk2 is a critical regulator of p53 function, given that cells derived from Chk2-deficient mice are defective in the transcriptional induction of p53 target genes at the G_1-S checkpoint [9–11]. In addition to the defect in

☆ *Abbreviations:* IR, ionizing radiation; FITC, fluorescein isothiocyanate.

* Corresponding author. Fax: +81 562 46 8437.
E-mail address: motoyama@nils.go.jp (N. Motoyama).

0006-291X/$ - see front matter © 2005 Elsevier Inc. All rights reserved.
doi:10.1016/j.bbrc.2005.05.126

transcriptional activation of proapoptotic genes such as those for Bax and Noxa, various cell types derived from Chk2-deficient mice, including thymocytes, neurons, and adenoviral E1A-transformed mouse embryonic fibroblasts, are resistant to the induction of p53-mediated apoptosis by IR [9–12].

Translocation of p53 to mitochondria and direct induction of apoptosis [13–16] as well as the p53-dependent release of histone H1.2 from the nucleus and consequent induction of apoptosis [17] have been recently described in cells exposed to IR, although the signaling pathway to leading these translocations remain unclear. Chk2 forms a stable complex with p53 in human cells [18] and phosphorylates human p53 at Ser^{20} (Ser^{23} in mouse) and COOH-terminal fragment including Ser^{366}, Ser^{378}, and Thr^{387} of human p53 [10,19–21]. These observations prompted us to examine whether Chk2 regulates the induction of such transcription-independent apoptosis by p53 and histone H1.2. We now show that the translocation of p53 and histone H1 to mitochondria is markedly reduced in Chk2-deficient cells as a result of the defect in p53 stabilization. We therefore conclude that Chk2 regulates both transcription-independent and transcription-dependent mechanisms of p53-mediated apoptosis by stabilizing p53 and by increasing its transcriptional regulatory activity.

Materials and methods

Mice. The generation of Chk2-deficient mice was described previously [9]. The endogenous and disrupted *Chk2* genes were detected by polymerase chain reaction analysis of mouse tail DNA either with 5′-CTCGCTGACCTAGGTAGCAGGACC-3′ and 5′-TGTGCCGG TAGAGGAGCTGG-3′ or with 5′-CTCGCTGACCTAGGTAGCAG GACC-3′ and 5′-GGGTGGGGTGGGATTAGATAAATG-3′ as primers, respectively. The amplification protocol comprised 35 cycles of denaturation for 1 min at 94 °C, annealing for 90 s at 64 °C, and elongation for 90 s at 72 °C. Mice deficient in p53 were obtained from Taconic (Taconic, Germantown, NY).

X-irradiation of cells. Freshly isolated thymocytes from mice of the indicated genotypes were suspended in RPMI 1640 medium supplemented with 10% fetal bovine serum. They were exposed to the indicated dose of X-radiation at a rate of 4.53 Gy/min and then cultured for the indicated times under a humidified atmosphere of 6% CO_2 at 37 °C.

Apoptosis assay. Apoptosis in irradiated thymocytes was assayed with the use of an Annexin V-FITC Apoptosis Detection Kit (Sigma, St. Louis, MO). In brief, harvested cells were washed with ice-cold phosphate-buffered saline, resuspended in 1× binding buffer [10 mM Hepes–NaOH (pH 7.5), 140 mM NaCl, and 2.5 mM $CaCl_2$] at a density of 1.0×10^6 cells/ml, and then incubated for 10 min with fluorescein isothiocyanate (FITC)-conjugated annexin V. The proportion of cells positive for staining by annexin V-FITC was determined immediately thereafter by flow cytometry with a FACScalibur instrument and data analysis with CELL Quest software (BD Pharmingen, San Diego, CA).

Immunoblot analysis. Cells were lysed in a solution containing 50 mM Hepes–NaOH (pH 8.0), 150 mM NaCl, 25 mM EGTA, 1 mM EDTA, 0.1% Tween 20, 10% glycerol, 0.1 M NaF, and a mixture of protease inhibitors (Complete-Mini; Roche, Mannheim, Germany). The protein concentration of the lysates was determined with the BCA protein assay reagent (Pierce, Rockford, IL), after which samples (10 μg of protein) were subjected to SDS–polyacrylamide gel electrophoresis and immunoblot analysis with mouse monoclonal antibodies to mouse p53 (IMX25; Novocastra, Newcastle, UK) or to γ-tubulin (GTU-88, Sigma) or with rabbit polyclonal antibodies to Puma (Pro-Sci, Poway, CA). Immune complexes were detected with horseradish peroxidase-conjugated secondary antibodies and the ECL Plus system (Amersham Bioscience, Piscataway, NJ).

Isolation of mitochondria. Mitochondria were isolated with the use of a Mitochondria/Cytosol Fractionation Kit (BioVision, Mountain View, CA). In brief, thymocytes were washed with ice-cold phosphate-buffered saline, resuspended in 1 ml of 1× cytosol extraction buffer mix containing dithiothreitol and protease inhibitor cocktail, and then incubated for 10 min on ice. The cells were disrupted by 60 strokes of a Dounce homogenizer to yield a crude extract, which was then centrifuged at 700*g* for 10 min at 4 °C. The resulting supernatant was centrifuged at 10,000*g* for 30 min at 4 °C, and the final pellet was washed twice with 1× cytosol extraction buffer mix and saved as the mitochondrial fraction. Protein concentration was determined with a Dc Protein Assay Kit (Bio-Rad, Hercules). The crude extract and mitochondrial fraction were solubilized in SDS sample buffer and then subjected to SDS–polyacrylamide gel electrophoresis and immunoblot analysis with mouse monoclonal antibodies to mouse p53 or to histone H1 (AE-4; Santa Cruz Biotechnology, Santa Cruz, CA). The purity of the mitochondrial fraction was assessed by immunoblot analysis with a mouse monoclonal antibody (20EB; Molecular Probes, Eugene OR) to OxPhos complex IV subunit IV (COX4) and rabbit polyclonal antibodies (FL-261, Santa Cruz Biotechnology) to proliferating cell nuclear antigen (PCNA), as markers for mitochondria and the nucleus, respectively.

Results and discussion

Accumulation of Puma and translocation of both p53 and histone H1 coincide with the initiation of apoptosis

The tumor suppressor p53 induces apoptosis by transcription-dependent and transcription-independent mechanisms in response to exposure of cells to IR. Although the transcriptional activation of p53 target genes for proapoptotic proteins such as Puma is relatively rapid, the accumulation of these proteins to a level sufficient to mediate apoptosis presumably requires additional time. We therefore first examined the kinetics both of the induction of apoptosis and of the expression of Puma in thymocytes exposed to IR. Apoptotic cells were detected 3 h after X-irradiation and their percentage increased thereafter (Fig. 1A). Although p53 was stabilized within 1 h after X-irradiation, Puma accumulation was not apparent until 3 h (Fig. 1B), indicating that the accumulation of Puma is coincident with the initiation of apoptosis. We next examined the kinetics of the translocation of p53 and histone H1 to mitochondria. Translocation of both p53 and histone H1 to mitochondria was detected 3 h after X-irradiation of thymocytes (Fig. 1C). Together, these results thus indicated that both transcription-dependent and transcription-independent pathways contribute to the initiation of p53-mediated apoptosis in thymocytes exposed to IR.

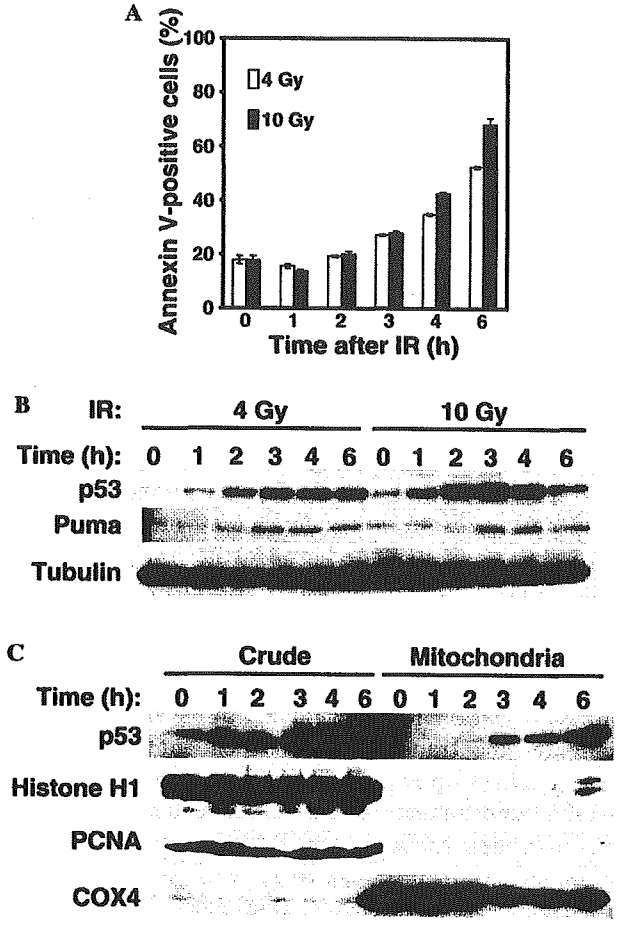

Fig. 1. Kinetics of apoptosis, Puma expression, and translocation of p53 and histone H1 to mitochondria in thymocytes exposed to IR. (A) Thymocytes from wild-type mice were exposed (or not) to 4 or 10 Gy of X-radiation and then cultured for the indicated times before staining with annexin V-FITC and determination of the percentage of annexin V-positive cells by flow cytometry. Data are means ± SD of triplicates from an experiment that was performed a total of two times with similar results. (B) Total cell lysates prepared from thymocytes at the indicated times after exposure to IR (4 or 10 Gy) were subjected to immunoblot analysis with antibodies to mouse p53, to Puma, and to γ-tubulin (loading control). (C) Mitochondrial fractions were purified from thymocytes at the indicated times after exposure to IR (10 Gy). Both total crude extracts (10 μg of protein) and purified mitochondria (10 μg of protein) were subjected to immunoblot analysis with antibodies to mouse p53, to histone H1, to PCNA, and to COX4.

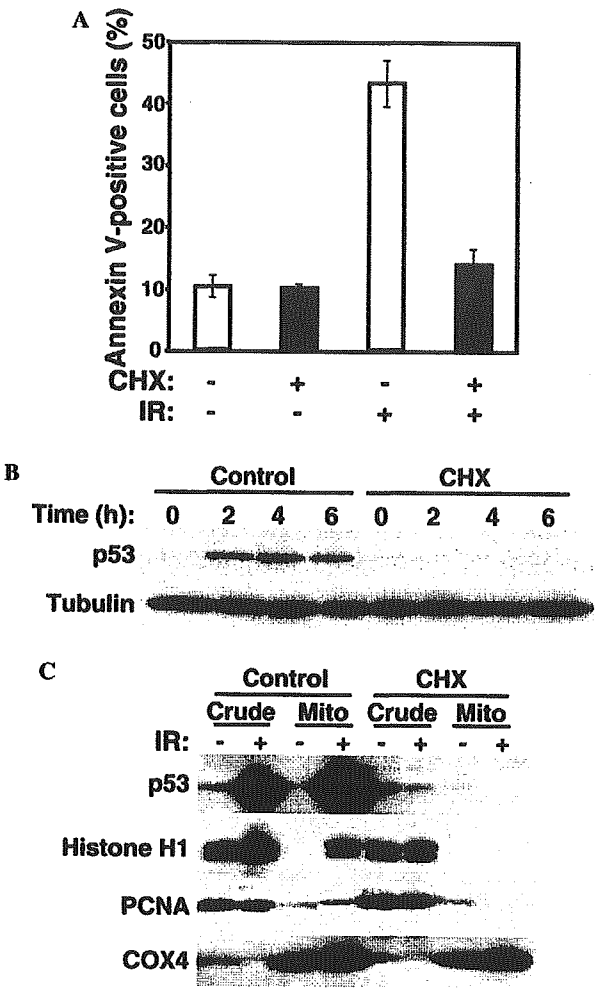

Fig. 2. Inhibitory effects of cycloheximide on p53 stabilization and apoptosis induced by IR. (A) Freshly isolated thymocytes from wild-type mice were incubated with or without cycloheximide (CHX, 10 μg/ml) for 30 min, exposed to 10 Gy of X-radiation, and incubated for an additional 5 h in the continued presence of cycloheximide. The cells were then stained with annexin V-FITC and analyzed by flow cytometry. Data are means ± SD of triplicates from an experiment that was performed a total of two times with similar results. (B) Thymocytes were treated with cycloheximide and irradiated as in (A) and were then lysed at the indicated times after irradiation. Whole cell extracts (10 μg of protein) were subjected to immunoblot analysis with antibodies to the indicated proteins. (C) Thymocytes from wild-type mice were treated with cycloheximide and irradiated as in (A). After incubation of the cells for an additional 4 h, mitochondria (Mito) were isolated and subjected together with total crude extracts (10 μg of protein in each case) to immunoblot analysis with antibodies to the indicated proteins.

Stabilization of p53 is essential for IR-induced histone H1 translocation and apoptosis

The previous observation that IR triggered apoptosis in E1A-transformed mouse embryonic fibroblasts in the presence of the protein synthesis inhibitor cycloheximide indicated that a latent p53 is able to induce apoptosis in a transcription-independent manner [12,22]. We therefore examined whether p53 also induces apoptosis in thymocytes in the presence of cycloheximide. Cycloheximide treatment inhibited the increase in the number of annexin V-positive cells induced by IR (Fig. 2A). The IR-induced accumulation of p53 in thymocytes was also prevented, with the amount of p53 actually decreasing to below the basal level, in cycloheximide-treated thymocytes (Fig. 2B). The amount of p53 protein is still high at basal level in E1A-transformed MEF compared to that of thymocytes in which p53 protein almost is not detectable. These observations indicate that in contrast to E1A-transformed MEFs, stabilization of p53 is essential for IR-induced apoptosis in thymocytes.

We next examined whether cycloheximide also inhibited the translocation of histone H1 to mitochondria in wild-type thymocytes. Isolation of mitochondria at this time revealed that the translocation of neither p53 nor histone H1 to mitochondria was apparent in the cycloheximide-treated cells (Fig. 2C). These data thus indicated that p53 stabilization is essential for the IR-induced translocation of both p53 and histone H1 to mitochondria as well as for IR-induced apoptosis.

Chk2 regulates p53 and histone H1 translocation by stabilizing p53

Thymocytes derived from Chk2-deficient mice were markedly resistant to the induction of apoptosis by IR compared with those from wild-type mice (Fig. 3A). To examine whether Chk2 also regulates the translocation of p53 and histone H1 to mitochondria in response to IR, we exposed thymocytes derived from wild-type or Chk2-deficient mice to X-radiation and isolated the mitochondrial fraction at various times thereafter. Immunoblot analysis revealed that irradiation of wild-type thymocytes increased both the amount of p53 in the crude extract and mitochondrial fraction as well as that of histone H1 in the mitochondrial fraction (Fig. 3B). In contrast, the IR-induced stabilization of p53 was impaired in Chk2-deficient thymocytes and the extent of the IR-induced translocation of both p53 and histone H1 to mitochondria was markedly reduced (Fig. 3B). Together, these results indicated that apoptosis mediated by translocation of p53 and histone H1 to mitochondria in response to IR is also impaired in Chk2-deficient thymocytes as a result of the defective stabilization of p53.

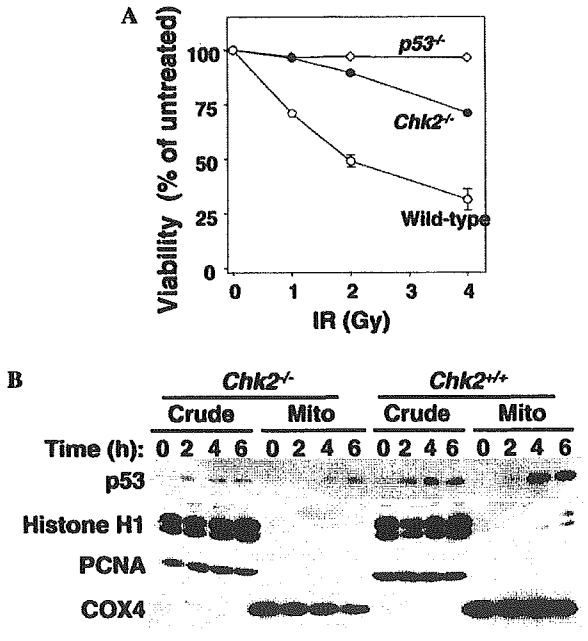

Fig. 3. Resistance to IR-induced apoptosis and impaired translocation of p53 and histone H1 to mitochondria in Chk2-deficient thymocytes. (A) Thymocytes derived from wild-type, Chk2-deficient, or p53-deficient mice were exposed to the indicated doses of X-radiation and incubated for 24 h and analysis by flow cytometry. Data are means ± SD of triplicates from an experiment that was performed a total of two times with similar results. (B) Mitochondrial fractions were isolated from thymocytes of wild-type or Chk2-deficient mice at the indicated times after exposure to IR (10 Gy). Both total crude extracts (10 μg of protein) and mitochondria (10 μg of protein) were subjected to immunoblot analysis with antibodies to the indicated antibodies.

The tumor suppressor protein p53 performs multiple functions related to cell cycle checkpoints, apoptosis, and cellular senescence [4,5]. Among these functions, induction of apoptosis has been thought to be the most important for suppression of tumorigenesis [6,7]. The p53 protein induces apoptosis by transcription-dependent and transcription-independent mechanisms [23], the latter being mediated by translocation of p53 and histone H1.2 to mitochondria [13–17]. It remains unknown whether posttranslational modification of p53 is required for its IR-induced mitochondrial translocation, although other functions of p53 are regulated by phosphorylation [8]. We have now shown that Chk2 regulates the transcription-independent mechanism of p53-mediated apoptosis as well as the transcription-dependent mechanism [9–11] in thymocytes exposed to IR. Although the amount of p53 that translocated to mitochondria in response to IR was greatly reduced in Chk2-deficient thymocytes, this effect appeared to be attributable to the lack of p53 stabilization in these cells rather than to a requirement of Chk2 for such translocation per se.

The p53 protein was previously shown to be required for the release of histone H1.2 from the nucleus in response to IR [17]. The IR-induced translocation of histone H1 to mitochondria was also reduced in extent in thymocytes derived from Chk2-deficient mice compared with that in wild-type cells. Furthermore, the amounts of p53 and histone H1 that translocated to mitochondria appeared well correlated with each other, suggesting that the stabilization (and translocation) of p53 determines the efficiency of histone H1 translocation. Together, our observations indicate that, in addition to its regulation of the transcription-dependent mechanism of p53-mediated apoptosis, Chk2 regulates IR-induced apoptosis in thymocytes by increasing the stability of p53, which in turn allows the translocation of accumulated p53 as well as that of histone H1 to mitochondria.

Genetic studies in mice have shown that Chk2 plays an important role in regulation of p53 functions, especially in the induction of apoptosis in response to IR [9–12]. Chk2 was recently shown to collaborate with Brca1 in tumorigenesis [24]. Brca1 has pleiotropic functions, contributing to homologous recombination repair [25], transcription-coupled repair [26], and activation of

the G_2-M cell cycle checkpoint [27,28]. Although the defective differentiation and proliferation of Brca1-deficient thymocytes are rescued by the defect in apoptosis conferred by deficiency of Chk2, the double deficiency leads to the onset of thymic lymphoma in mice [24]. Our present data therefore indicate that Chk2 functions as a tumor suppressor by regulating both transcription-dependent and transcription-independent mechanisms of p53-mediated apoptosis.

Acknowledgments

We thank member of Geriatric Research for discussions. This work was supported by a Grant-in-Aid for Scientific Research on Priority Areas from the Ministry of Education, Culture, Sports, Science, and Technology of Japan, Health Sciences Research Grants for Comprehensive Research on Aging and Health from the Ministry of Health, Labour, and Welfare of Japan and Takeda Science Foundation.

References

[1] B.B. Zhou, S.J. Elledge, The DNA damage response: putting checkpoints in perspective, Nature 408 (2000) 433–439.
[2] Y. Shiloh, ATM and related protein kinases: safeguarding genome integrity, Nat. Rev. Cancer 3 (2003) 155–168.
[3] N. Motoyama, K. Naka, DNA damage tumor suppressor genes and genomic instability, Curr. Opin. Genet. Dev. 14 (2004) 11–16.
[4] D.P. Lane, Cancer. p53, guardian of the genome, Nature 358 (1992) 15–16.
[5] A.J. Levine, p53, the cellular gatekeeper for growth and division, Cell 88 (1997) 323–331.
[6] C.A. Schmitt, J.S. Fridman, M. Yang, E. Baranov, R.M. Hoffman, S.W. Lowe, Dissecting p53 tumor suppressor functions in vivo, Cancer Cell 1 (2002) 289–298.
[7] H. Symonds, L. Krall, L. Remington, M. Saenz-Robles, S. Lowe, T. Jacks, T. Van Dyke, p53-dependent apoptosis suppresses tumor growth and progression in vivo, Cell 78 (1994) 703–711.
[8] E. Appella, C.W. Anderson, Post-translational modifications and activation of p53 by genotoxic stresses, Eur. J. Biochem. 268 (2001) 2764–2772.
[9] H. Takai, K. Naka, Y. Okada, M. Watanabe, N. Harada, S. Saito, C.W. Anderson, E. Appella, M. Nakanishi, H. Suzuki, K. Nagashima, H. Sawa, K. Ikeda, N. Motoyama, Chk2-deficient mice exhibit radioresistance and defective p53-mediated transcription, EMBO J. 21 (2002) 5195–5205.
[10] A. Hirao, Y.Y. Kong, S. Matsuoka, A. Wakeham, J. Ruland, H. Yoshida, D. Liu, S.J. Elledge, T.W. Mak, DNA damage-induced activation of p53 by the checkpoint kinase Chk2, Science 287 (2000) 1824–1827.
[11] A. Hirao, A. Cheung, G. Duncan, P.M. Girard, A.J. Elia, A. Wakeham, H. Okada, T. Sarkissian, J.A. Wong, T. Sakai, E. De Stanchina, R.G. Bristow, T. Suda, S.W. Lowe, P.A. Jeggo, S.J. Elledge, T.W. Mak, Chk2 is a tumor suppressor that regulates apoptosis in both an ataxia telangiectasia mutated (ATM)-dependent and an ATM-independent manner, Mol. Cell. Biol. 22 (2002) 6521–6532.
[12] M.T. Jack, R.A. Woo, A. Hirao, A. Cheung, T.W. Mak, P.W. Lee, Chk2 is dispensable for p53-mediated G1 arrest but is required for a latent p53-mediated apoptotic response, Proc. Natl. Acad. Sci. USA 99 (2002) 9825–9829.
[13] M. Mihara, S. Erster, A. Zaika, O. Petrenko, T. Chittenden, P. Pancoska, U.M. Moll, p53 has a direct apoptogenic role at the mitochondria, Mol. Cell 11 (2003) 577–590.
[14] P. Dumont, J.I. Leu, A.C. Della Pietra 3rd, D.L. George, M. Murphy, The codon 72 polymorphic variants of p53 have markedly different apoptotic potential, Nat. Genet. 33 (2003) 357–365.
[15] J.E. Chipuk, T. Kuwana, L. Bouchier-Hayes, N.M. Droin, D.D. Newmeyer, M. Schuler, D.R. Green, Direct activation of Bax by p53 mediates mitochondrial membrane permeabilization and apoptosis, Science 303 (2004) 1010–1014.
[16] J.I. Leu, P. Dumont, M. Hafey, M.E. Murphy, D.L. George, Mitochondrial p53 activates Bak and causes disruption of a Bak-Mcl1 complex, Nat. Cell Biol. 6 (2004) 443–450.
[17] A. Konishi, S. Shimizu, J. Hirota, T. Takao, Y. Fan, Y. Matsuoka, L. Zhang, Y. Yoneda, Y. Fujii, A.I. Skoultchi, Y. Tsujimoto, Involvement of histone H1.2 in apoptosis induced by DNA double-strand breaks, Cell 114 (2003) 673–688.
[18] J. Falck, C. Lukas, M. Protopopova, J. Lukas, G. Selivanova, J. Bartek, Functional impact of concomitant versus alternative defects in the Chk2-p53 tumour suppressor pathway, Oncogene 20 (2001) 5503–5510.
[19] N.H. Chehab, A. Malikzay, M. Appel, T.D. Halazonetis, Chk2/hCds1 functions as a DNA damage checkpoint in G(1) by stabilizing p53, Genes Dev. 14 (2000) 278–288.
[20] S.Y. Shieh, J. Ahn, K. Tamai, Y. Taya, C. Prives, The human homologs of checkpoint kinases Chk1 and Cds1 (Chk2) phosphorylate p53 at multiple DNA damage-inducible sites, Genes Dev. 14 (2000) 289–300.
[21] Y.H. Ou, P.H. Chung, T.P. Sun, S.Y. Shieh, p53 C-terminal phosphorylation by CHK1 and CHK2 participates in the regulation of DNA-damage-induced C-terminal acetylation, Mol. Biol. Cell (2005).
[22] R.A. Woo, M.T. Jack, Y. Xu, S. Burma, D.J. Chen, P.W. Lee, DNA damage-induced apoptosis requires the DNA-dependent protein kinase, and is mediated by the latent population of p53, EMBO J. 21 (2002) 3000–3008.
[23] J.J. Manfredi, p53 and apoptosis: it's not just in the nucleus anymore, Mol. Cell 11 (2003) 552–554.
[24] J.P. McPherson, B. Lemmers, A. Hirao, A. Hakem, J. Abraham, E. Migon, E. Matysiak-Zablocki, L. Tamblyn, O. Sanchez-Sweatman, R. Khokha, J. Squire, M.P. Hande, T.W. Mak, R. Hakem, Collaboration of Brca1 and Chk2 in tumorigenesis, Genes Dev. 18 (2004) 1144–1153.
[25] M.E. Moynahan, J.W. Chiu, B.H. Koller, M. Jasin, Brca1 controls homology-directed DNA repair, Mol. Cell 4 (1999) 511–518.
[26] L.C. Gowen, A.V. Avrutskaya, A.M. Latour, B.H. Koller, S.A. Leadon, BRCA1 required for transcription-coupled repair of oxidative DNA damage, Science 281 (1998) 1009–1012.
[27] J.S. Larson, J.L. Tonkinson, M.T. Lai, A BRCA1 mutant alters G2-M cell cycle control in human mammary epithelial cells, Cancer Res. 57 (1997) 3351–3355.
[28] X. Xu, Z. Weaver, S.P. Linke, C. Li, J. Gotay, X.W. Wang, C.C. Harris, T. Ried, C.X. Deng, Centrosome amplification and a defective G2-M cell cycle checkpoint induce genetic instability in BRCA1 exon 11 isoform-deficient cells, Mol. Cell 3 (1999) 389–395.

MOLECULAR AND CELLULAR BIOLOGY, Nov. 2005, p. 9469–9477 Vol. 25, No. 21
0270-7306/05/$08.00+0 doi:10.1128/MCB.25.21.9469–9477.2005

A-Kinase-Anchoring Protein 95 Functions as a Potential Carrier for the Nuclear Translocation of Active Caspase 3 through an Enzyme-Substrate-Like Association

Shinji Kamada,[1,2,3]* Ushio Kikkawa,[2] Yoshihide Tsujimoto,[3] and Tony Hunter[1]*

Molecular and Cell Biology Laboratory, The Salk Institute, La Jolla, California[1]; Biosignal Research Center, Kobe University, Kobe, Japan[2]; and Laboratory of Molecular Genetics, Osaka University Medical School and Graduate School of Medicine, Suita, Osaka, Japan[3]

Received 29 June 2005/Accepted 5 August 2005

Caspase-mediated proteolysis is a critical and central element of the apoptotic process, and caspase 3, one of the effector caspases, is proposed to play essential roles in the nuclear morphological changes of apoptotic cells. Although many substrates for caspase 3 localize in the nucleus and caspase 3 translocates from the cytoplasm to the nuclei after activation in apoptotic cells, the molecular mechanisms of nuclear translocation of active caspase 3 have been unclear. Recently, we suggested that a substrate-like protein(s) served as a carrier to transport caspase 3 from the cytoplasm into the nucleus. In the present study, we identified A-kinase-anchoring protein 95 (AKAP95) as a caspase 3-binding protein. Small interfering RNA-mediated depletion of AKAP95 reduced apoptotic nuclear morphological changes, suggesting that AKAP95 is involved in the process of apoptotic nuclear morphological changes. The association of AKAP95 with active caspase 3 was analogous to an enzyme-substrate interaction. Furthermore, overexpression of AKAP95 with nuclear localization sequence mutations inhibited nuclear morphological changes in apoptotic cells. These results indicate that AKAP95 is a potential carrier protein for active caspase 3 from the cytoplasm into the nuclei in apoptotic cells.

Apoptosis plays important roles in a variety of biological events, including morphogenesis, maintenance of tissue homeostasis, and removal of harmful cells. Apoptosis is morphologically characterized by chromatin condensation, nuclear fragmentation, and formation of membrane-enclosed vesicles called apoptotic bodies, which are phagocytosed by other cells. Caspases, a family of cysteine proteases, are required for apoptosis execution (2, 11, 12, 39). Caspase 3, one of the effector caspases, has been implicated as a key mediator of apoptosis in mammalian cells (11, 12, 39) and plays essential roles in the nuclear changes in apoptotic cells (25, 43, 44) despite the cytoplasmic localization of the precursor form of caspase 3 (28, 34). In addition, although many nuclear substrates for caspase 3 have been identified (11, 12, 18, 39), the precise localization of active caspase 3 in apoptotic cells had been unclear. Recently, we confirmed the nuclear localization of active caspase 3 in apoptotic cells by using antibodies specific for the large and small subunits of active caspase 3 (22). Furthermore, we showed that the nuclear translocation of caspase 3 required its proteolytic activation and substrate recognition, whereas caspase 7, another effector caspase, was not translocated into the nuclei (22). These results suggested that the nuclear translocation of active caspase 3 is not mediated by passive diffusion but requires an active transport system and that active caspase 3 may be translocated in association with a substrate-like protein(s) from the cytoplasm into the nucleus in apoptotic cells.

A-kinase-anchoring proteins (AKAPs) bind to the regulatory subunit of cyclic AMP-dependent protein kinase (PKA) to direct the kinase to discrete intracellular locations (10). A 95-kDa AKAP, designated AKAP95, has been identified from human (692 amino acids), mouse (687 amino acids), and rat (687 amino acids) sources (8, 14). AKAP95 proteins are highly conserved among species, with human AKAP95 showing 78% identity (85% similarity) with mouse and rat AKAP95. AKAP95 contains several characteristic sequences, including a nuclear matrix targeting site, overlapping putative bipartite nuclear localization sequences (NLSs), two zinc fingers, and a type II PKA regulatory subunit (RII) binding domain (see Fig. 5A), and is suggested to be localized to the nuclear matrix (1, 8, 14). Recently, it was reported that AKAP95 plays an essential role in chromatin condensation during mitosis through the anchoring of a cyclic AMP/PKA-signaling complex and the recruitment of components of the condensin complex onto chromatin (9, 13, 36).

To identify a substrate-like protein(s) that might serve as carrier proteins to transport active caspase 3 from the cytoplasm into nucleus in apoptotic cells, we used a cloning method for caspase substrates that uses the yeast two-hybrid system (21). In this manner, we identified AKAP95 as a caspase 3-binding protein and obtained evidence that AKAP95 functions as a carrier protein for the nuclear translocation of active caspase 3.

* Corresponding author. Mailing address for Shinji Kamada: Biosignal Research Center, Kobe University, 1-1 Rokkodai-cho, Nada-ku, Kobe 657-8501, Japan. Phone: 81-78-803-5965. Fax: 81-78-803-5972. E-mail: skamada@kobe-u.ac.jp. Mailing address for Tony Hunter: Molecular and Cell Biology Laboratory, The Salk Institute, 10010 North Torrey Pines Rd., La Jolla, CA 92037. Phone: (858) 453-4100. Fax: (858) 457-4765. E-mail: hunter@salk.edu.

MATERIALS AND METHODS

Cell culture and apoptosis induction. HepG2 and Jurkat cells were cultured in RPMI 1640 medium with 10% fetal bovine serum. HeLa (clone D98AH2) and 293T cells were cultured in Dulbecco modified Eagle medium supplemented with 10% fetal bovine serum. For induction of apoptosis, HepG2 cells were

treated with 1 μg of an agonistic anti-Fas antibody (CH-11; Kamiya Biomedical Company)/ml in the presence of 0.2 μg of actinomycin D/ml or with 200 μg of etoposide/ml. Transfection was performed using Lipofectamine (Life Technologies) for 293T cells and GenePORTER 2 (Gene Therapy Systems) for HepG2 cells according to the manufacturer's instructions.

Antibodies and immunoprecipitation. Preparation of anti-active caspase 3 polyclonal antibodies (antibody 2622) and anti-active caspase 3 monoclonal antibody (clone CS-1) was described elsewhere (22). Anti-caspase 3 monoclonal antibody (C31720) and anti-AKAP95 monoclonal antibody (A74220) were obtained from Transduction Laboratories; anti-caspase 3 polyclonal antibodies (sc-1224) and anti-lamin B1 polyclonal antibodies (sc-6217) were from Santa Cruz Biotechnology; anti-AKAP95 polyclonal antibodies (06-417) were from Upstate Biotechnology, Inc.; anti-caspase 3 polyclonal antibodies (antibody 9662) were from Cell Signaling Technology; anti-green fluorescent protein (anti-GFP) monoclonal antibody (antibody 8371) was from Clontech; anti-GFP polyclonal antibodies (A-6455) were from Molecular Probes; anti-Xpress monoclonal antibody (R910-25) was from Invitrogen; and anti-α-tubulin monoclonal antibody (T-5168) was from Sigma. The anti-AKAP95 rabbit antiserum used for immunoprecipitation experiments was kindly provided by J. D. Scott.

For immunoprecipitation experiments, cells were lysed in lysis buffer (10 mM Tris-HCl [pH 7.5], 150 mM NaCl, 5 mM EDTA, 0.4% Nonidet P-40, 2 μg of aprotinin/ml, 2 μg of leupeptin/ml, 1 μg of pepstatin/ml, 100 μg of phenylmethylsulfonyl fluoride/ml). Lysates were incubated with anti-AKAP95 serum or normal rabbit serum for 1 h at 4°C with constant rotation and then with 5% (vol/vol) protein A-agarose for an additional 1 h. Cell lysates and immunoprecipitates were separated by sodium dodecyl sulfate-polyacrylamide gel electrophoresis (SDS-PAGE) and immunoblotted with the indicated antibodies.

siRNA experiments. Synthetic 21-nucleotide double-stranded RNAs were obtained from Dharmacon Research. The targeting sequence of human AKAP95 was AACTACAATTACTATGGCGCC, corresponding to coding nucleotides 100 to 120 relative to the first nucleotide of the start codon. HepG2 cells were transfected with Oligofectamine reagent (Invitrogen). One day before transfection, cells were seeded at a density of 9×10^5 cells per 10-cm dishes. In a first tube, 600 μl of Opti-MEM was mixed with 36 μl of 20 μM small interfering RNA (siRNA) duplex. In a second tube, 144 μl of Opti-MEM was incubated with 36 μl of Oligofectamine for 10 min at room temperature. The two mixtures above were combined, gently mixed, and incubated for 20 min at room temperature. After addition of 384 μl of Opti-MEM to the mixture, the entire mixture was added to the cells, followed by incubation for 4 days.

Yeast two-hybrid assays. The yeast reporter strain L40 (*MATa trp1 leu2 his3 ade2 LYS2::lexA-HIS3 URA3::lexA-lacZ*) was used as the host, and cells positive for growth on selective medium (-His/-Leu/-Trp) were examined for β-galactosidase activity using a colony filter-lift assay.

Plasmid constructions. Construction of pBTM-casp3-p12p17^m and pBTM-casp3-p12 was described previously (21). A fragment encoding caspase 3-p17^m was generated by PCR using caspase 3 cDNA bearing the C163S mutation as a template and was cloned into the EcoRI site of pBTM$_{116}$ to generate pBTM-casp3-p17^m. A fragment encoding caspase 3-p12^m was generated by PCR using pcasp3-R207E-GFP plasmid (22) as a template and cloned into the EcoRI-BamHI site of pBTM-casp3-p12p17^m lacking the caspase 3-p12 to generate pBTM-casp3-p12^{m}p17^m. pGAD-AKAP95 (clone 13 6-687) was originally identified as a possible substrate for caspase 3 by yeast two-hybrid screening (21) and contained residues 6 to 687 of mouse AKAP95. Various deletion mutants of AKAP95 for yeast two-hybrid assays were constructed by using suitable restriction enzyme sites or PCR. To substitute Glu^{675} for Gly and Thr^{677} for Gly, a PCR method using mutagenic oligonucleotide primers was used.

Construction of pCAG-casp3, pcasp3-Wt-GFP, pcasp7-Wt-GFP, pcasp3-C163S-GFP, pcasp3-D175A-GFP, pcasp3-R64E-GFP, and pcasp3-R207E-GFP was described elsewhere (22). The prodomain deletion mutant of caspase 3 was constructed by PCR and cloned into the EcoRI-BamHI site of pEGFP-C1 (Clontech) to generate pGFP-Δpro-casp3-Wt. The C-terminally hemagglutinin (HA)-tagged procaspase 3 cDNA fragment was cloned into the EcoRI site of pUC-CAGGS (29) to generate pCAG-casp3-HA. To construct caspase 3 expression plasmids as a fusion to the N terminus of DsRed (3), the fragment encoding caspase 3 was cloned into the EcoRI-BamHI site of pDsRed1-N1 (Clontech) to generate pcasp3-Wt-DsRed.

The human AKAP95 cDNA (kindly provided by K. Tasken) was cloned into the XhoI site of pUC-CAGGS, the BamHI site of pcDNA3.1/His A (Invitrogen) and the XhoI site of pEGFP-C2 (Clontech) to generate pCAG-AKAP95-Wt, pcDNA-AKAP95-Wt and pGFP-AKAP95-Wt. To substitute Arg^{290} for Ser, Lys^{304} for Asn, Arg^{305} for Ser, and Thr^{681} for Gly, a PCR method using mutagenic oligonucleotide primers was used. The human AKAP95 cDNAs containing mutations at R290S, K304N/R305S, R209S/K304N/R305S, T681G, and R209S/K304N/R305S/T681G were cloned into pEGFP-C2 to generate pGFP-AKAP95-1M, pGFP-AKAP95-2M, pGFP-AKAP95-3M, pGFP-AKAP95-Wt-T681G, and pGFP-AKAP95-3M-T681G.

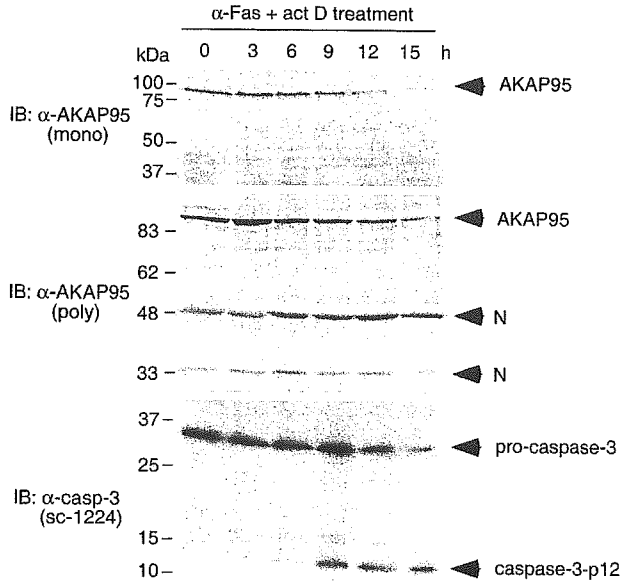

FIG. 1. AKAP95 is not a substrate for caspase 3 in vivo. HepG2 cells were treated with an agonistic anti-Fas antibody in the presence of actinomycin D for the indicated periods. Cell lysates were subjected to SDS-PAGE and immunoblotted with anti-AKAP95 monoclonal antibody, anti-AKAP95 polyclonal antibodies, or anti-caspase 3 polyclonal antibodies (sc-1224; Santa Cruz Biotechnology) that detect both procaspase 3 and caspase 3-p12 as indicated. N, nonspecific band.

RESULTS

Identification of caspase 3-binding proteins is valuable for understanding the molecular mechanisms of apoptotic execution. Therefore, we used the yeast two-hybrid method, which has been successfully used to identify caspase substrates (21, 30). In this manner, we identified several potential caspase 3 substrates including gelsolin (clones 1, 9, and 12 in reference 21), and a potential binding protein to caspase 3 (clone 13 in reference 21). Clone 13 contained residues 6 to 687 of mouse AKAP95, which has bipartite NLSs (see Fig. 5A) and is suggested to play an essential role in chromatin condensation during mitosis (9, 13, 36).

AKAP95 is a caspase 3-binding protein. AKAP95 (clone 13 in reference 21) was not cleaved completely in in vitro cleavage assays even though it has three tetrapeptides DNSD^{90}, DCRD^{175}, and DLCD^{349}, which fit the consensus caspase 3 cleavage sequence, whereas gelsolin (clones 1, 9, and 12 in reference 21) was cleaved completely. These results suggested that AKAP95 is not a good substrate for caspase 3. Therefore, we examined whether AKAP95 is a substrate for caspase 3 in vivo by using anti-AKAP95 monoclonal or polyclonal antibodies, which were prepared against C-terminal fragments of AKAP95. After treatment of HepG2 cells with an agonistic anti-Fas antibody, procaspase 3 was cleaved and activated (Fig. 1, lower panel). However, although the levels of AKAP95 protein gradually decreased, specific AKAP95 cleavage products were not detected by immunoblotting with an

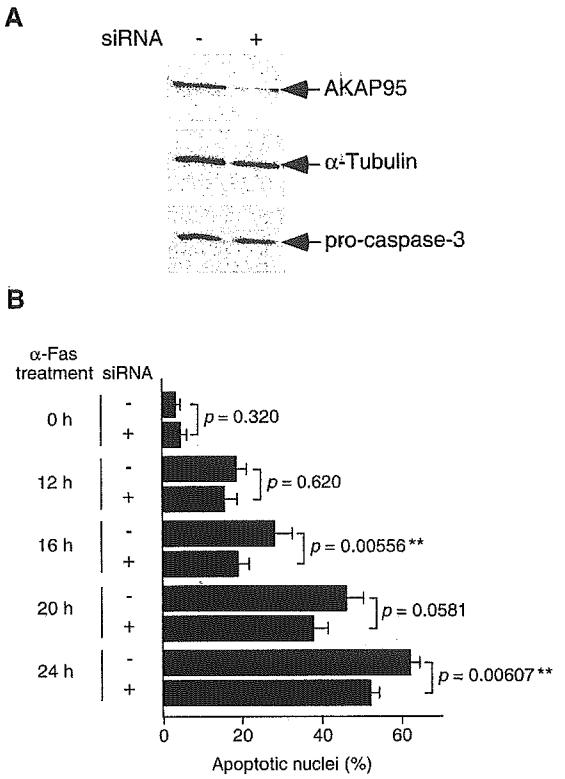

FIG. 2. Inhibition of nuclear morphological changes of apoptotic cells by siRNA for AKAP95. (A) Lysates from HepG2 cells transfected with or without siRNA for AKAP95 for 4 days were fractionated by SDS-PAGE and immunoblotted with anti-AKAP95 polyclonal antibodies, anti-α-tubulin monoclonal antibody, or anti-caspase 3 monoclonal antibody. (B) HepG2 cells transfected with or without siRNA for AKAP95 were treated with an agonistic anti-Fas antibody in the presence of actinomycin D for the indicated periods and collected and fixed with 3.7% formaldehyde for 10 min. After staining with Hoechst 33342, the percentage of the cells showing apoptotic nuclei to the total cells was measured. At least 100 cells were counted for each measurement in all experiments. The data (mean ± the standard deviation) were obtained from at least three independent experiments. Significant test results (P values) are shown. **, $P < 0.01$.

anti-AKAP95 monoclonal (Fig. 1, upper panel) or polyclonal (Fig. 1, middle panel) antibodies during apoptosis. These results suggested that AKAP95 is probably not a substrate for caspase 3 in vivo and lacks a cleavage site in the interaction domain.

AKAP95 plays a role in apoptotic nuclear morphological changes. To investigate a possible role for AKAP95 in apoptotic execution, we examined the effects of AKAP95 overexpression in cells. However, we did not observe any differences between transfected and nontransfected cells (data not shown and see Fig. 5B). As an alternative means of determining whether AKAP95 plays a role in apoptosis, we used siRNA (15) to deplete AKAP95 protein in HepG2 cells (Fig. 2). At 4 days after transfection of siRNA for AKAP95, the level of AKAP95 was decreased significantly (to <15%), whereas the levels of α-tubulin and procaspase 3 were unaffected (Fig. 2A). Therefore, the same number of cells transfected with siRNA for AKAP95 were reseeded, and apoptosis was induced by treatment with anti-Fas antibody. HepG2 cells transfected with siRNA for AKAP95 exhibited delayed nuclear morphological changes compared to control cells (Fig. 2B), suggesting that AKAP95 plays a role(s) in the nuclear morphological changes of apoptotic cells.

Association of caspase 3 with AKAP95 in yeast. Recently, we proposed that active caspase 3 is translocated in association with a substrate-like protein(s) from the cytoplasm into the nucleus in apoptotic cells (22). A carrier protein for the nuclear translocation of active caspase 3 would not be expected to be a caspase substrate per se because a typical enzyme-substrate complex is not stable but rather should associate reasonably stably with caspase 3 and should have a functional NLS. AKAP95 has all of these properties and therefore is a candidate for a carrier protein of caspase 3. To investigate this possibility, we next defined the AKAP95-binding region in caspase 3 using direct yeast two-hybrid assays (Table 1). Cotransformation of pBTM-casp3-p12p17^m, which expresses both p17 containing C163S mutation and p12 subunits of caspase 3, and pGAD-AKAP95 (clone 13 6-687) yielded His$^+$ transformants that were also β-galactosidase positive. However, neither caspase 3-p12 nor caspase 3-p17^m alone was able to bind to AKAP95, indicating that both subunits of caspase 3 are required for its binding to AKAP95. Furthermore, the R207E mutation, which prevents recognition of the P3 amino acid of substrates by caspase 3 (32, 42) and inhibited the nuclear translocation of active caspase 3 (22), abolished the association with AKAP95. These results suggest that the interaction of caspase 3 and AKAP95 may be analogous to an enzyme-substrate interaction.

TABLE 1. Association of AKAP95 with active caspase 3 in yeast two-hybrid assays[a]

pGAD (Gal4 AD)[b]	pBTM (LexA BD)[c]	β-Galactosidase activity[d]
AKAP95 (#13 6-687)	casp3-p12p17^m	+
AKAP95 (#13 6-687)	casp3-p12^{m}p17^m	−
AKAP95 (#13 6-687)	casp3-p17^m	−
AKAP95 (#13 6-687)	casp3-p12	−
AKAP95 (#13 6-47)	casp3-p12p17^m	−
AKAP95 (#13 6-341)	casp3-p12p17^m	−
AKAP95 (#13 6-542)	casp3-p12p17^m	−
AKAP95 (#13 340-429)	casp3-p12p17^m	−
AKAP95 (#13 428-687)	casp3-p12p17^m	+
AKAP95 (#13 544-687)	casp3-p12p17^m	+
AKAP95 (#13 544-670)	casp3-p12p17^m	−
AKAP95 (#13 556-687)	casp3-p12p17^m	+
AKAP95 (#13 556-679)	casp3-p12p17^m	+
AKAP95 (#13 544-687 E675G)	casp3-p12p17^m	−
AKAP95 (#13 544-687 T677G)	casp3-p12p17^m	−

[a] Yeast L40 cells were cotransfected with expression plasmids for Gal4 activation domain (Gal4 AD) fusion proteins and for LexA DNA-binding domain (LexA BD) fusion proteins as indicated.

[b] "#13" represents the clone number that was originally identified by yeast two-hybrid screening (21). The numbers (6-687, etc.) correspond to the encoded amino acids of AKAP95.

[c] pBTM-casp3-p12p17^m was used for expression of caspase 3-p12 and caspase 3-p17(C163S), pBTM-casp3-p12^{m}p17^m was used for expression of caspase 3-p12(R207E) and caspase 3-p17(C163S), pBTM-casp3-p17^m was used for expression of caspase 3-p17(C163S), and pBTM-casp3-p12 was used for expression of caspase 3-p12.

[d] Each transformation mixture was plated on a synthetic dropout plate lacking leucine, tryptophan, and histidine. Filter assays for β-galactosidase activity were performed to detect interactions between fusion proteins. +, development of blue color within 2 h; −, no growth of transformed yeast colonies.

Next we defined the active caspase 3-binding region in AKAP95 using yeast two-hybrid assays (Table 1). Various deletion mutants of AKAP95 were fused to the Gal4 activation domain and transformed into yeast with pBTM-casp3-p12p17^{m}. Cotransformation of pGAD-AKAP95 (clone 13, 544-687) or pGAD-AKAP95 (clone 13, 556-679), but not pGAD-AKAP95 (clone 13, 544-670), with pBTM-casp3-p12p17^{m} conferred the His^{+} phenotype and β-galactosidase activity, indicating that the binding site of AKAP95 for active caspase 3 is present in the C-terminal region (amino acids 556 to 679) of AKAP95 and that amino acids 671 to 679 are required for association with active caspase 3 in yeast. Although a consensus caspase 3 cleavage sequence (DXXD) was not found in this region, the tetrapeptide ($E^{675}QTG^{678}$), which is related to the caspase 3 cleavage site in gelsolin (DQTD) (21), is present (see Fig. 5C). To test whether this sequence is essential for binding to active caspase 3, we constructed E675G and T677G point mutants in a C-terminal fragment of mouse AKAP95 (amino acids 544 to 687). These mutations abolished the interaction of AKAP95 with active caspase 3 in yeast, suggesting that the $E^{675}QTG^{678}$ sequence in AKAP95 is required for binding to active caspase 3, possibly because this sequence functions as a noncleavable pseudosubstrate site for caspase 3. The fact that nuclear translocation of active caspase 3 did not require Arg^{64} or Cys^{163} (22), both of which are essential for recognition of, and cleavage after, Asp at P1 position (32, 42), is consistent with the absence of Asp at the position corresponding to P1 in the EQTG active caspase 3 binding site of mouse AKAP95.

Association of caspase 3 with AKAP95 in vivo. Next we tested whether an in vivo association between active caspase 3 and AKAP95 could be detected by coimmunoprecipitation. GFP-tagged caspase 3 with or without mutations was transiently overexpressed in 293T cells together with human AKAP95. As a control for specificity, C-terminally GFP-tagged procaspase 7 was coexpressed with AKAP95. Even though the cells were not induced to undergo apoptosis, casp3-Wt-GFP, GFP-Δpro-casp3-Wt, and casp7-Wt-GFP were proteolytically activated, presumably as a result a stress, such as serum starvation or a toxic effect of liposomes during transfection, or the overexpression of the wild-type caspases (Fig. 3A, upper panel). After immunoprecipitation of AKAP95, coprecipitated GFP-fusion proteins were detected with anti-GFP antibody (Fig. 3A, middle panel). Proteolytically activated casp3-p12-GFP derived from casp3-Wt-GFP and GFP-casp3-p17 derived from GFP-Δpro-casp3-Wt, but not casp7-p12-GFP from casp7-Wt-GFP, were coprecipitated with AKAP95, suggesting that active caspase 3 interacts with AKAP95 in vivo and that the association of effector caspases with AKAP95 may be specific for caspase 3. These results are consistent with our findings that caspase 3, but not caspase 7, translocated from the cytoplasm to the nucleus in apoptotic cells (22). Interestingly, all of the unprocessed GFP-caspase fusion proteins were coprecipitated along with AKAP95, but the level of casp7-Wt-GFP precipitated was significantly less than that of casp3-Wt-GFP. Since the coprecipitation of N-terminally GFP-tagged caspase 3 with AKAP95 was less effective than that of C-terminally GFP tagged caspase 3, GFP fused to the N terminus of caspase 3-p17 may interfere with immunocomplex formation.

To further analyze the interaction between procaspase 3 and AKAP95 in vivo, immunoprecipitations were carried out from lysates of 293T cells that were transiently transfected with AKAP95 and procaspase 3 expression plasmids (Fig. 3B). Procaspase 3 and C-terminally HA- or DsRed-tagged pro-caspase 3 was coprecipitated with AKAP95, suggesting that procaspase 3 also interacts with AKAP95 in 293T cells.

We also tested whether coprecipitation of AKAP95 with caspase 3 could be detected. For this purpose, N-terminally His-tagged AKAP95 was transiently overexpressed in 293T cells together with C-terminally GFP-tagged procaspase 3, and GFP-tagged caspase 3 was immunoprecipitated with anti-GFP antibodies, followed by detection of coprecipitated His-tagged AKAP95 by immunoblotting with anti-Xpress monoclonal antibody. As shown in Fig. 3C, His-tagged AKAP95 was coprecipitated with GFP-tagged caspase 3, although we could not determine whether His-tagged AKAP95 was coprecipitated with GFP-tagged procaspase 3, caspase 3-p12, or both.

To determine whether association between endogenous AKAP95 and caspase 3 proteins could be detected, lysates from HepG2 cells treated with or without anti-Fas antibody were separated into supernatant and pellet fractions after lysis with digitonin and immunoprecipitated with anti-AKAP95 serum, followed by immunoblotting with anti-caspase 3 antibodies. When we used anti-caspase 3 polyclonal antibodies for immunoblotting, which recognize both procaspase 3 and caspase 3-p12 subunit (Fig. 1), no active caspase 3 coprecipitating with AKAP95 was detected (data not shown). However, we detected a low level (<1%) of procaspase 3 coprecipitating with AKAP95 in the supernatant fraction of normal cells by using anti-caspase 3 monoclonal antibody in immunoblotting (Fig. 3D), suggesting that AKAP95 interacts with procaspase 3 endogenously in the cytoplasm of normal cells.

Colocalization of active caspase 3 and AKAP95. If AKAP95 functions as a carrier protein to transport active caspase 3 from the cytoplasm into nucleus, AKAP95 is expected to localize to the cytoplasm in normal cells and colocalize with active caspase 3 in apoptotic nuclei. To test this, various human cell lines were fractionated into supernatant and pellet fractions after lysis with digitonin, using lamin B1 as a nuclear marker. As shown in Fig. 4A, procaspase 3 was present only in the supernatant fraction, and AKAP95 was present in both the pellet and the supernatant fractions from normal cells. Next, apoptotic HepG2 cells were fractionated into supernatant and pellet fractions (Fig. 4B, left panel). Although procaspase 3 was present in the supernatant fraction, the caspase 3-p17 subunit and AKAP95 were present in both the pellet and supernatant fractions. Furthermore, HepG2 cells were stained with anti-AKAP95 and anti-active caspase 3 antibodies after treatment with anti-Fas antibody or etoposide (Fig. 4B, right panel). Although AKAP95 was detected in both nuclei and cytoplasm, active caspase 3 was not detected in cells before induction of apoptosis. However, AKAP95 and active caspase 3 were both highly enriched in the region around condensed nuclei in apoptotic cells, indicating colocalization of active caspase 3 and AKAP95 in apoptotic cells.

Function of AKAP95 in apoptotic nuclear morphological changes. If AKAP95 functions to carry caspase 3 from the cytoplasm into the nucleus, overexpression of AKAP95 with NLS-inactivating mutations should inhibit nuclear translocation of

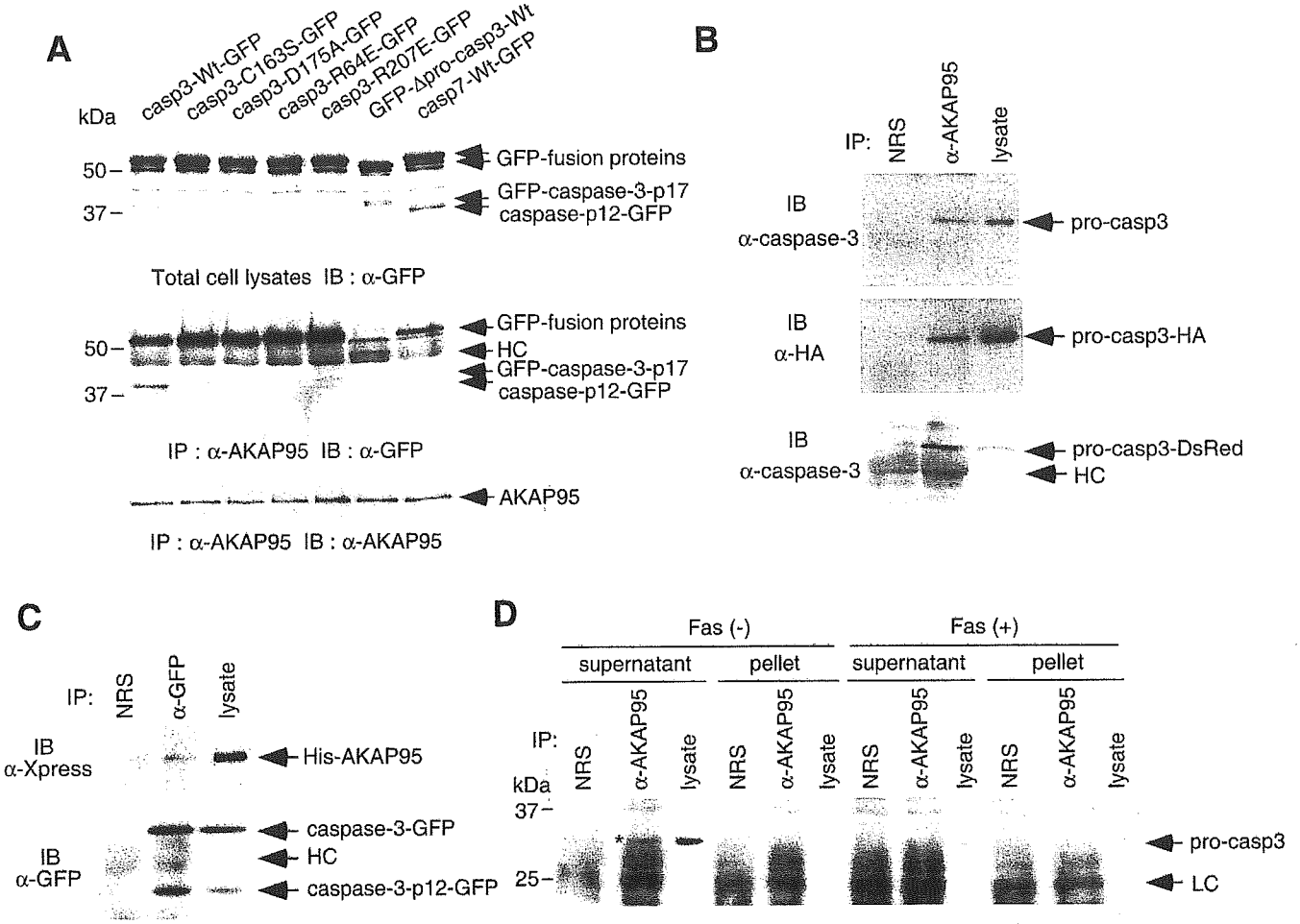

FIG. 3. In vivo association of caspase 3 with AKAP95. (A) Active caspase 3, but not active caspase-7, binds to AKAP95. 293T cells were transfected with caspase-GFP expression plasmids as indicated, together with pCAG-AKAP95-Wt. Casp3-C163S-GFP contained the mutation at the catalytic Cys, casp3-D175A-GFP contained the cleavage site mutation between the p17 and p12 subunits, casp3-R64E-GFP and casp3-R207E-GFP contained the mutations of substrate recognition sites, and GFP-Δpro-casp3-Wt was a prodomain deletion mutant. After incubation for 24 h, lysates were immunoprecipitated with anti-AKAP95 serum. The input lysates (upper panel) and the immunoprecipitates (middle and lower panels) were fractionated by SDS-PAGE and immunoblotted with anti-GFP monoclonal antibody (upper and middle panels) or anti-AKAP95 monoclonal antibody (lower panel). HC, heavy chain. (B) Coprecipitation of procaspase 3 with AKAP95 in transiently overexpressed 293T cells. Lysates from 293T cells transfected with either pCAG-casp3, pCAG-casp3-HA, or pcasp3-Wt-DsRed, together with pCAG-AKAP95-Wt, were immunoprecipitated with normal rabbit serum (NRS) or anti-AKAP95 serum (α-AKAP95). The immunoprecipitates and the input lysates were fractionated by SDS-PAGE and immunoblotted with anti-caspase 3 monoclonal antibody (upper and lower panels) or anti-HA monoclonal antibody (12CA5) (middle panel). (C) Coprecipitation of AKAP95 with caspase 3 in transiently overexpressed 293T cells. Lysates from 293T cells transfected pcDNA-AKAP95-Wt together with pcasp3-Wt-GFP were immunoprecipitated with normal rabbit serum (NRS) or anti-GFP polyclonal antibodies (α-GFP). The immunoprecipitates and the input lysates were fractionated by SDS-PAGE and immunoblotted with anti-Xpress monoclonal antibody that recognizes the leader peptide from the pcDNA3.1/His vector between His tag and AKAP95 (upper panel) or anti-GFP monoclonal antibody (lower panel). (D) Procaspase 3 binds to AKAP95 at endogenous protein levels. HepG2 cells treated with or without an agonistic anti-Fas antibody in the presence of actinomycin D for 12 h were divided into supernatant or pellet fractions after lysis with digitonin and immunoprecipitated as described in panel B. The immunoprecipitates and the input lysates were fractionated by SDS-PAGE and immunoblotted with anti-caspase 3 monoclonal antibody. The asterisk indicates the procaspase 3 coprecipitated with AKAP95. LC, light chain.

active caspase 3 by sequestration in the cytoplasm and thus prevent nuclear morphological changes in apoptotic cells. AKAP95 has potential overlapping bipartite NLSs (Fig. 5A) at amino acids 289 to 305 and amino acids 290 to 306. To identify amino acids necessary for the nuclear translocation of AKAP95, we constructed point mutants of basic amino acids in the putative NLS of human AKAP95 and fused these mutants to the C terminus of GFP. Mutation of Arg^{290} to Ser in AKAP95 (AKAP95-1M) had no effect on the nuclear localization of GFP-AKAP95 fusion protein (Fig. 5B), whereas a double mutation of Lys^{304} to Asn and Arg^{305} to Ser (AKAP95-2M) dramatically impaired nuclear accumulation of the fusion protein. Furthermore, combined mutation of R290S/K304N/R305S (AKAP95-3M) completely prevented nuclear localization of the AKAP95-GFP fusion protein (Fig. 5B). These results indicated that the overlapping bipartite NLSs located at amino acids 289 to 306 are essential for the nuclear import of AKAP95. Furthermore, introduction of the T681G point mutation (T677G in mouse AKAP95) (Table 1 and